Gondwana Research 20 (2011) 309–324

Contents lists available at ScienceDirect

Gondwana Research

journal homepage: www.elsevier.com/locate/gr

Tectonothermal evolution and exhumation history of the Paleozoic Proto-Andean Gondwana margin crust: The Famatinian Belt in NW Argentina

C.R. de los Hoyos [a,*], A.P. Willner [b], M.A. Larrovere [c,d], J.N. Rossi [a], A.J. Toselli [a], M.A.S. Basei [e]

[a] INSUGEO-CONICET, Miguel Lillo 205, 4000, San Miguel de Tucumán, Argentina
[b] Institut für Geologie, Mineralogie & Geophysik, Ruhr-Universität, D-44780 Bochum, Germany
[c] Departamento de Geociencias, CRILAR-CONICET, Entre Ríos y Mendoza s/n, 5301, Anillaco, La Rioja, Argentina
[d] Universidad Nacional de La Rioja, Av. Dr. René Favaloro, 5300, La Rioja, Argentina
[e] Instituto de Geociências, Universidade de São Paulo, Rua do Lago 562, 05508-080, São Paulo, Brazil

ARTICLE INFO

Article history:
Received 20 April 2010
Received in revised form 10 December 2010
Accepted 10 December 2010
Available online 25 December 2010

Handling Editor: E. Tohver

Keywords:
Geothermobarometry
Geochronology
Exhumation history
Famatinian Belt
Altiplano–Puna-like orogen

ABSTRACT

We studied the P–T–t evolution of a mid-crustal igneous-metamorphic segment of the Famatinian Belt in the eastern sector of the Sierra de Velasco during its exhumation to the upper crust. Thermobarometric and geochronological methods combined with field observations permit us to distinguish three tectonic levels. The deepest Level I is represented by metasedimentary xenoliths and characterized by prograde isobaric heating at 20–25 km depth. Early/Middle Ordovician granites that contain xenoliths of Level I intruded in the shallower Level II. The latter is characterized by migmatization coeval with granitic intrusions and a retrograde isobaric cooling P–T path at 14–18 km depth. Level II was exhumed to the shallowest supracrustal Level III, where it was intruded by cordierite-bearing granites during the Middle/Late Ordovician and its host-rock was locally affected by high temperature–low pressure HT/LP metamorphism at 8–10 km depth. Level III was eventually intruded by Early Carboniferous granites after long-term slow exhumation to 6–7 km depth. Early/Middle Ordovician exhumation of Level II to Level III (Exhumation Period I, 0.25–0.78 mm/yr) was faster than exhumation of Level III from the Middle/Late Ordovician to the Lower Carboniferous (Exhumation Period II, 0.01–0.09 mm/yr). Slow exhumation rates and the lack of regional evidence of tectonic exhumation suggest that erosion was the main exhumation mechanism of the Famatinian Belt. Widespread slow exhumation associated with crustal thickening under a HT regime suggests that the Famatinian Belt represents the middle crust of an ancient Altiplano–Puna-like orogen. This thermally weakened over-thickened Famatinian crust was slowly exhumed mainly by erosion during ~180 Myr.

1. Introduction

Unravelling the exhumation history of rocks in different geodynamic settings has become a major focus of recent research in petrology since exhumation processes reflect the evolution of the orogen and have great influence on the formation of orogenic topography (Ring et al., 1999). Fossil orogens are exhumed relics of crustal segments which frequently contain a comprehensive record of petrogenetic processes such as deformation, metamorphism, magmatism, and partial melting as well as the pressure–temperature–time (P–T–t) paths that rocks underwent during the orogenic period (e.g. Brown, 2010; Maruyama et al., 2010). The study of the P–T evolution and exhumation history of a fossil orogen provides direct insights into geodynamic processes and exhumation mechanisms of crustal rocks. The Famatinian Belt represents the middle- to upper crust of a fossil Andean-type orogen, which developed along the proto-Pacific margin of Gondwana in Paleozoic times. Several interpretations about the origin and evolution of the magmatism (e.g. Rapela et al., 1992; Toselli et al., 1996; Saavedra et al., 1998; Pankhurst et al., 1998, 2000; Rossi et al., 2002), and the metamorphic evolution of the Famatinian Belt (e.g. Vujovich, 1994; Dahlquist and Baldo, 1996; Hauzenberger et al., 2001; Lucassen and Becchio, 2003; Büttner et al., 2005; Otamendi et al., 2008; Larrovere et al., 2011) were proposed from petrologic studies in different outcropping crustal segments along this orogen. The tectonic scenario in which the Famatinian crust evolved has been envisaged in two contrasting models: (1) significant back-arc extensional shearing and crustal thinning (e.g. Büttner et al., 2005; Büttner, 2009) and (2) strong compression and crustal thickening (e.g. Willner et al., 1987; Whitmeyer and Simpson, 2004) although both models invoke high heat input by magmatic advection from the upper mantle to explain high T/P conditions. Ordovician high T back-arc extension has been interpreted from P–T–d (deformation)–t paths and shear-indicator kinematic analysis in the migmatitic basement assuming tilting of the present-day shear zone orientations during the Andean orogeny (Büttner et al., 2005; Büttner, 2009), coeval deposition of thick marine sediments over this basement (Büttner, 2009) and generation of

* Corresponding author. Fax: +54 3827 494231.
E-mail address: punkamilo@hotmail.com (C.R. de los Hoyos).

1342-937X/$ – see front matter © 2010 International Association for Gondwana Research. Published by Elsevier B.V. All rights reserved.
doi:10.1016/j.gr.2010.12.004

ferrosilicic (high iron and silica) magmas which would have ascended from a deep cold diapir or mantle wedge plume (Fernández et al., 2008). Ordovician high T compression has been proposed on the basis of kinematic analysis using the present-day orientation of shear zones and associated evidence of strong shortening (e.g. tight folding) throughout the migmatite basement (Willner et al., 1987; Whitmeyer and Simpson, 2004; Wegmann et al., 2008). The exhumation history (rates and mechanisms) of different segments of the Famatinian Belt, which would yield additional information about geodynamic processes and extensional/compressional tectonic regimes along this orogen, was not yet addressed.

The Sierra de Velasco is located in the zone between the main arc and the back arc of the Famatinian Belt. It constitutes a key area to study exhumation rates since outcrops representing magmatic and metamorphic events from different crustal levels which occurred in different geologic time are exposed. This paper is aimed at providing information on the timing of mid- and supracrustal magmatic and metamorphic events in the eastern sector of the Sierra de Velasco. We combined new and previously published results from monazite and zircon dating, thermobarometry and field data to calculate exhumation rates and infer possible exhumation mechanisms.

2. Geologic setting

2.1. The Famatinian Belt

The Famatinian Belt is a Paleozoic subduction-related continental magmatic arc and its metasedimentary host-rocks formed during the Famatinian Orogenic Cycle along the proto-Andean margin of Gondwana (Aceñolaza and Toselli, 1973). The middle to upper crust of this orogen crops out along a N–S trending belt of at least 800 km length and 400 km width and form the Paleozoic basement of the Sierras Pampeanas in central and NW-Argentina (Fig. 1a). The Famatinian metasedimentary basement is broadly composed of psammopelitic high temperature medium/low pressure migmatite and subordinated lower grade phyllite and schist. Evidence of strong folding and ductile west-directed reverse shearing parallel to the migmatitic layering is widely observed (e.g. Willner et al., 1987; Büttner et al., 2005; Larrovere et al., 2008; Büttner, 2009). This high-T compressive deformation took place during an episode of crustal thickening which occurred probably in Cambrian and Early Ordovician times (Willner et al., 1987). Similar peak metamorphic conditions in migmatite (650–800 °C and 4–7 kbar) were calculated in different regions of the Famatinian Belt such as the Sierras de Quilmes (Büttner et al., 2005), Ancasti–Ambato–Aconquija (Larrovere et al., 2011), Valle Fértil–La Huerta (Otamendi et al., 2008) and San Luis (Delpino et al., 2007), suggesting that similar deepest paleo-depths of the Famatinian crust are exposed over a wide area. U–Pb and Sm–Nd ages of the high-T metamorphism throughout the orogen are ~530–500 Ma and ~470–440 Ma and overlap spatially (Pankhurst et al., 1998; Lucassen et al., 2000; Lucassen and Becchio, 2003; Büttner et al., 2005), indicating long-lived both high-T conditions within the Famatinian crust and subduction along western Gondwana. The Famatinian magmatic arc comprises two main NNW–SSE trending belts dominated by calc-alkaline granitic rocks (Pankhurst et al., 2000), a metaluminous I-type belt in the west, and a peraluminous S-type belt in the east (Fig. 1a). Intrusion of both granitic belts occurred from the Early to the Middle/Late Ordovician (~490–450 Ma; e.g. Rapela et al., 1992; Saavedra et al., 1998; Pankhurst et al., 1998, 2000; Büttner et al., 2005; Steenken et al., 2006), indicating that orogen-scale high-T metamorphism and plutonic activity were broadly coeval (e.g. Pankhurst et al., 2000; Rossi et al., 2002).

Ordovician Famatinian rocks were cut by numerous NNW–SSE trending east-dipping shear belts characterized by reverse west-directed thrusting (e.g. López and Toselli, 1993; Le Corre and Rossello, 1994). Geochronological evidence from syn-kinematic minerals suggests that these belts were active in Silurian and Devonian times. In the westernmost part of the Famatinian Belt, $^{40}Ar/^{39}Ar$ ages of medium-grade shear zones are around 430 Ma (Castro de Machuca et al., 2008). Medium- to low-grade brittle–ductile shear zones central part of the Famatinian Belt were still active in the Early Devonian (Sm/Nd isochron in garnet of ~400 Ma; Höckenreiner et al., 2003). It suggests that compressive tectonics was long-lived and accompanied the exhumation of the Famatinian crust. After a long period (~100 Myr) of reduced magmatism, widespread intrusion of post-tectonic supra-crustal granitic plutons occurred in the Devonian/Carboniferous (340–360 Ma; Grosse et al., 2009 and references therein). The minimum age of final exhumation of the Famatinian crust is indicated by Devonian/Carboniferous sediments overlying Ordovician metamorphic and granitic rocks as well as Carboniferous plutons at various locations (Lucassen et al., 2000; Pieroni and Georgieff, 2007).

Although it is broadly accepted that the Famatinian Belt is a subduction-related orogen (e.g. Toselli et al., 1996; Pankhurst et al., 1998), a Central Andean-type scenario was recently proposed by Lucassen and Franz (2005). They found striking similarities between the Cenozoic Altiplano–Puna plateau and the Famatinian Belt such as: (a) the widely distributed Ordovician migmatite basement of the Famatinian Belt exposing maximal paleo-depths of ~25 km may be a fossil analogue of the wide zone of partially melted rocks at ~15–25 km depth represented by the present-day seismic Altiplano Low-Velocity Zone (ALVZ; e.g. Heit et al., 2008); (b) widespread felsic calc-alkaline arc magmatism without significant mantle contribution in both orogens; and (c) lack of tectonically exhumed deep crustal high-pressure rocks (e.g. eclogites and blueschists). This Cenozoic–Paleozoic tectonic analogy is further discussed in Section 8.3.

Based on the across-arc tectonic subdivision of Otamendi et al. (2008) of the Famatinian Belt, we distinguish the fore-arc zone characterized by an accretionary wedge along the western side of the Sierra de Valle Fértil (Vujovich, 1994) and Famatina, the main arc zone including major batholiths such as the Sierras de Velasco and Chepes and the back-arc zone located east from the main arc and including the Sierras de Aconquija, Ambato, Ancasti and San Luis. Within this context the study area is located in the easternmost side of the main Famatinian arc.

2.2. The Sierra de Velasco

The Sierra de Velasco constitutes one of the most complete records of magmatic activity in the middle to upper crust during the Famatinian Orogeny. It is mainly composed of metaluminous and peraluminous Ordovician granitoids intruded by Carboniferous post-tectonic plutons (Fig. 1b). The pre-magmatic metasedimentary host-rock is present as small outcrops along the eastern flank of the Sierra and is classically referred as the southern equivalent of the La Cébila Formation (LCF) of the Sierra de Ambato (e.g. González Bonorino, 1951; Verdecchia and Baldo, 2010). The I-/S-type limit is represented in the central-southern sector of the Sierra de Velasco (Bellos, 2005). Thermobarometric studies in Ordovician plutons of the western flank of the Sierra de Velasco indicate emplacement in the middle crust (~5–6 kbar; Rossi et al., 2005; Rossi and Toselli, 2005). Cordierite-bearing granitoids are observed as small bodies spatially associated with the S-type belt (Fig. 1b), although they also intruded metaluminous I-type granodiorites in the Sierra de Chepes at upper-crustal levels in Ordovician times (Dahlquist et al., 2005). U–Pb ages obtained in the Sierra de Velasco and adjacent sectors indicate that the I- and S-type magmatism occurred in the Early to Middle Ordovician (~480–460 Ma; e.g. Pankhurst et al., 2000; Rapela et al., 2001; Dahlquist et al., 2008). The Ordovician granitoids were deformed by inverse shear represented by NNW–SSE trending belts crosscutting the Sierra (Rossi et al., 1999; Bellos, 2005). Lithological continuity on both sides of the shear zones suggests that relative movement of the blocks was relatively small and did not juxtapose different crustal segments. Early Carboniferous post-tectonic granites intruded the Ordovician

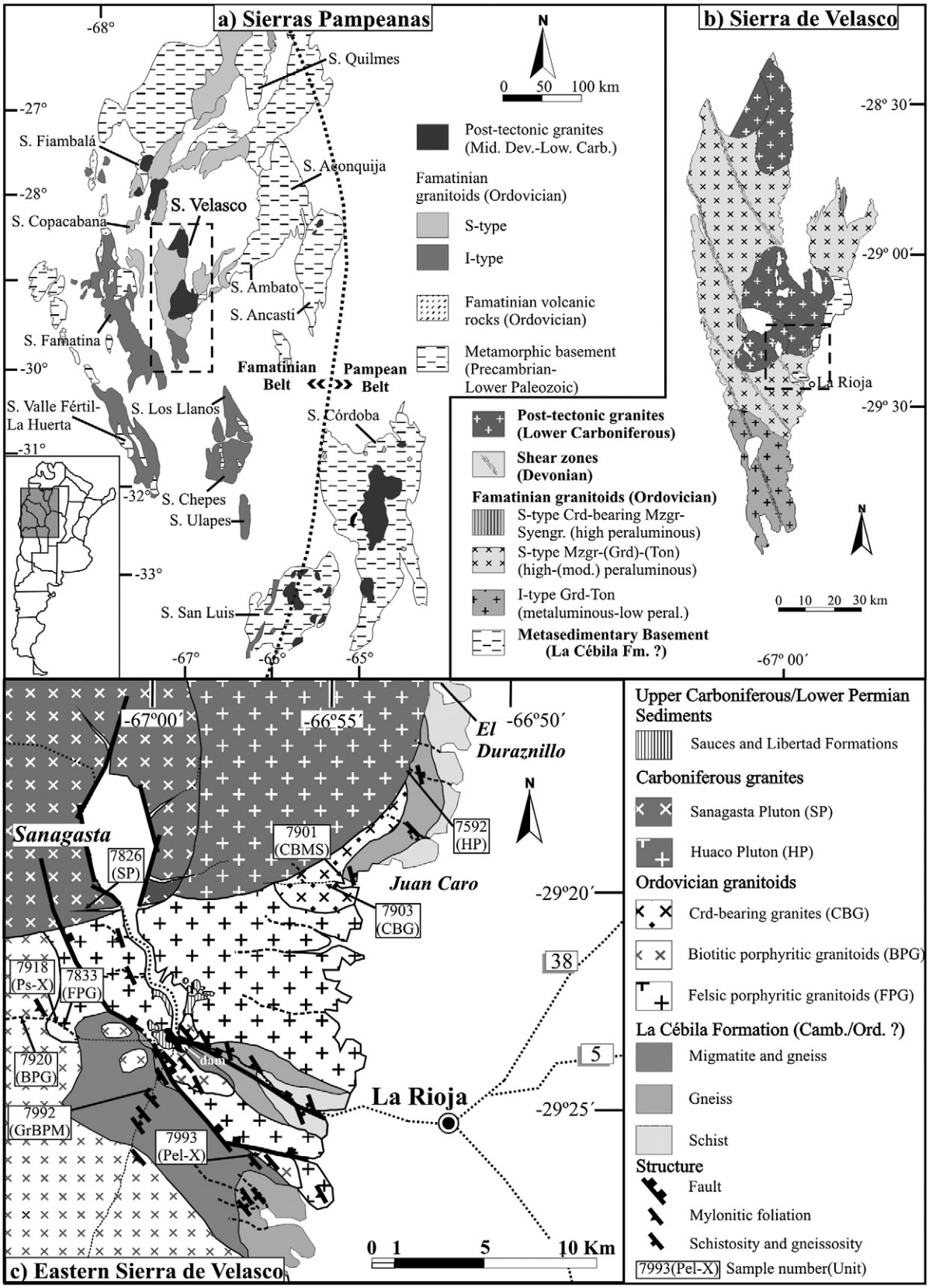

Fig. 1. Geological map of (a) the Famatinian belt in the Sierras Pampeanas geological province, (b) the Sierra de Velasco and (c) the eastern sector of the sierra (our study area). Panels (a) and (b) are modified from Grosse et al. (2009).

ones and cross-cut the shear zones (~360–340 Ma; Fig. 1b e.g. Grosse and Sardi, 2005; Dahlquist et al., 2006; Grosse et al., 2009). Late Carboniferous/ Early Permian continental sedimentary rocks of the Libertad and Sauces Formations overlie Ordovician and Carboniferous granites in the central-eastern sector of the sierra (Pieroni and Georgieff, 2007), constraining the time of complete exhumation of

Famatinian igneous and metamorphic rocks. Our study-area is located in the eastern flank of the Sierra de Velasco.

2.3. Field relationships

The host-rock of the study area is La Cébila Formation (LCF), which is dominated by migmatite in the southern region (W and SW of La Rioja) and schist and gneiss in the northern region (between El Duraznillo and Juan Caro) (Fig. 1c). The LCF shows tight folds with NNW–SSE trending and subvertical axial planes, the projection of the latter defining the schistosity and gneissosity of this unit. Strongly folded schist and gneiss xenoliths included in Ordovician mid-crustal plutons indicate the pre-magmatic character of this structure whereas migmatization appears to be syn-magmatic. The southern region of the study area consists of migmatite, gneiss and minor schist, intruded by partially deformed S-type granitoids (Fig. 1c). The migmatite is dominant and frequently contains garnet is regarded as garnet-bearing pelitic migmatite (GrBPM). The GrBPM mostly consists of stromatitic- and ptygmatic-type metatexite (Fig. 2 a, b), which show development of leucosomes parallel to the pre-migmatitic stage NNW–SSE trending schistosity and gneissosity. The leucosome/mesosome ratio is generally low, suggesting low melt fractions and incipient migmatization. The GrBPM frequently show intercalated gneiss- and schist-domains where partial melting seems not to be present. Schist and gneiss commonly show cm-scale compositional banding parallel to quartzite beds probably inherited from sedimentary bedding. Two Ordovician igneous bodies intruding the GrBPM were recognized; the felsic porphyritic granitoids (FPG) and the biotitic porphyritic granitoids (BPG). The FPG contain monzogranite and granodiorite with megacrysts of perthitic microcline and abundant microgranular enclaves and dm- to m-scale partially migmatized xenoliths near the intrusive contact (Fig. 2c). The BPG comprise dark-coloured biotitic granodiorite with megacrysts of perthitic microcline and minor plagioclase (Fig. 2d). Contacts with the FPG are rather diffuse. The younger age of the BPG is indicated by small bodies of biotite-rich porphyritic granodiorite indistinctly intruding both the FPG and the GrBPM. Contacts with the GrBPM are irregular to diffuse and textural transition is commonly observed, indicating coeval migmatization and intrusion (Fig. 2e).

The northern region of the study area consists of micaceous schist and gneiss frequently showing compositional banding, intruded by cordierite-bearing granites (CBG). Euhedral prisms of cordierite and sillimanite become abundant near the granitic intrusives. Meter-scale metapelitic septa and roof-pendants commonly contain finer-grained massive cordierite- and sillimanite-bearing hornfels. The CBG are represented by a small body composed of virtually undeformed granite with variable amounts of cordierite and sillimanite. Contacts with the host-rock and septa are sharp without migmatization (Fig. 2f). Angular xenoliths of porphyritic shear deformed granitoids very similar to the FPG within the CBG indicate intrusion of the latter into the former.

Evidence of the CBG intruding the FPG suggests that the southern and the northern region are not isolated blocks from different crustal levels, but an igneous-metamorphic crustal segment which evolved from the middle- to the upper crust. Thus, the southern region of the study area contains field evidence (e.g. diffuse and transitional intrusive contacts, migmatitic fabrics of the host-rock with garnet–sillimanite assemblages) of relatively deep coeval pre-Carboniferous igneous-metamorphic activity. The northern region exhibits clear features (e.g. sharp intrusive contacts, angular igneous and metasedimentary xenoliths, cordierite–sillimanite assemblages in the host-rock) of supra-crustal igneous-metamorphic overprint. Both regions of the study area were intruded by the Early Carboniferous Huaco and Sanagasta Plutons with sharp contacts.

3. Petrography and mineral chemistry

We chose metasedimentary rocks associated with Ordovician plutons since they contain mineral assemblages adequate for thermobarometry. The chosen lithologies to represent the relatively deep southern part are mesosome and leucosome of the GrBPM (samples 7992mes and 7992leu), a pelitic-gneiss xenolith (Pel-X; sample 7993) within the BPG and a metapsammite xenolith (Ps-X sample 7918) within the FPG (Fig. 1c). The chosen litho-type to represent shallower contact metamorphism of the northern region is a Crd-bearing metapelite

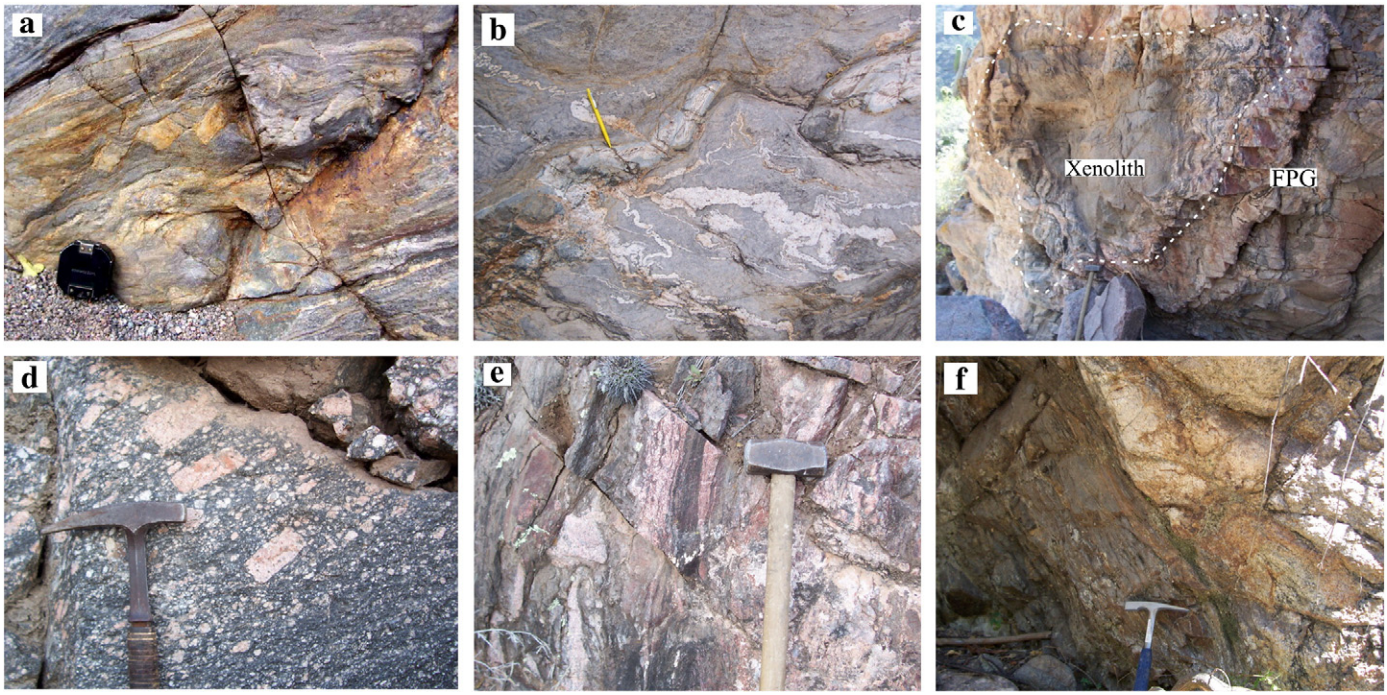

Fig. 2. Meso-scale stromatic (a) and ptygmatic (b) structures in the GrBPM. (c) Partially migmatized metasedimentary xenolith (outlined by dashed lines) in the FPG. (d) Outcrop aspect of the BPG and its migmatized contact with the GrBPM (e). (f) Sharp contact between the CBG and a metasedimentary roof-pendant.

septa (CBMS; sample 7901). Mineral abbreviations are according to recommendations by the IUGS (Siivola and Schmid, 2007). The analytical methods and data are available in the electronic supplementary file (Appendix A).

3.1. Samples 7992mes and 7992leu: GrBPM

This garnet-bearing stromatitic metatexite shows a well-defined compositional layering composed of 1–5 cm thick grey-coloured mica-rich mesosomes, 0.5–3 cm (occasionally up to 7 cm) Qtz-Pl-Grt-rich and mica-poor leucosomes, and 0.1–0.5 cm Bt-Sil rich melanosomes (Fig. 3a). A leucosome lens (sample 7992leu) and a mesosome band (sample 7992mes) were separated for petrographic and mineral–chemical studies. No relevant chemical difference between minerals within mesosome and leucosome is observed.

The mesosome is medium grained and contains quartz, plagioclase, biotite, white mica, garnet, prismatic and fibrous sillimanite, titanite, apatite, zircon, monazite, ilmenite and rutile. Micas within the mesosome are generally poorly aligned and define a week foliation parallel to the migmatitic layering. The leucosome is quartz-, plagioclase- and more garnet-rich, medium grained and contains the same minerals as the mesosome, although abundances and textures are markedly different. It shows neither foliation nor mica alignment. Plagioclase in both domains is typically unzoned and oligoclase in composition (An_{21-28}; see supplementary table in the electronic Appendix A). Sillimanite in leucosome and mesosome is only present as fibrolite replacing micas and as needle-shaped inclusions in garnet. Garnet occurs as isolated nearly idioblastic grains in the mesosome, whereas in the leucosome it shows resorbed boundaries and tends to amalgamate (Fig. 3b). Garnet in both domains is almandine ($Alm_{72-78}Grs_{1-4}Prp_{9-14}Sps_{8-13}$, see supplementary table in the electronic Appendix A) and exhibits diffusion-driven zoning patterns for spessartine, almandine and pyrope (Fig. 4a, b), even the largest grains. Grains of ~6.0 mm preserve some of their prograde pattern for grossular, whereas in smaller grains (~0.6 mm) the grossular pattern is almost parallel to the spessartine one. Large grains contain numerous inclusions of quartz, biotite, white mica (Fig. 3c), sillimanite needles, monazite and ilmenite. Fractures in garnet and biotite are occasionally filled with quartz veins. Biotite included in garnet cores shows slightly higher X_{Fe} [Fe/(Fe + Mg)] than biotite within garnet rims and matrix (see supplementary table in the electronic Appendix A). White mica is characterized by low Si content (6.09–6.11 a.p.f.u., O = 22).

3.2. Sample 7993: pelitic-gneiss xenolith in the BPG (Pel-X)

The rock is medium grained and contains quartz, biotite, white mica, plagioclase, garnet, sillimanite, ilmenite and zircon. The sample shows schistosity defined by alignment of micas and mm-scale compositional layering defined by lens-shaped and irregular quartz-rich leucocratic domains and biotite rich melanocratic domains.

Garnet abundance is low (<2%) and it is restricted to the micaceous domains, coexisting with sillimanite (Fig. 3d). Grains normally are inclusion-free, although some of them include very small grains of quartz, biotite and white mica. Small grains (~100 μm) are almandine, virtually grossular-free ($Alm_{66-71}Grs_{0}Prp_{13-17}Sps_{12-16}$; see supplementary table in the electronic Appendix A) and unzoned (Fig. 4d). Coarser blasts (~250 μm) show "bell-shaped" growth-zoning pattern with high-spessartine cores ($Alm_{53-61}Grs_{0-1}Prp_{5-10}Sps_{28-40}$), suggesting preserved prograde zoning (Fig. 4c). Rims seem to have been affected by thermal diffusive cation exchange. Plagioclase in both domains is unzoned and oligoclase in composition (An_{12-17}). Biotite exhibits a narrow range for

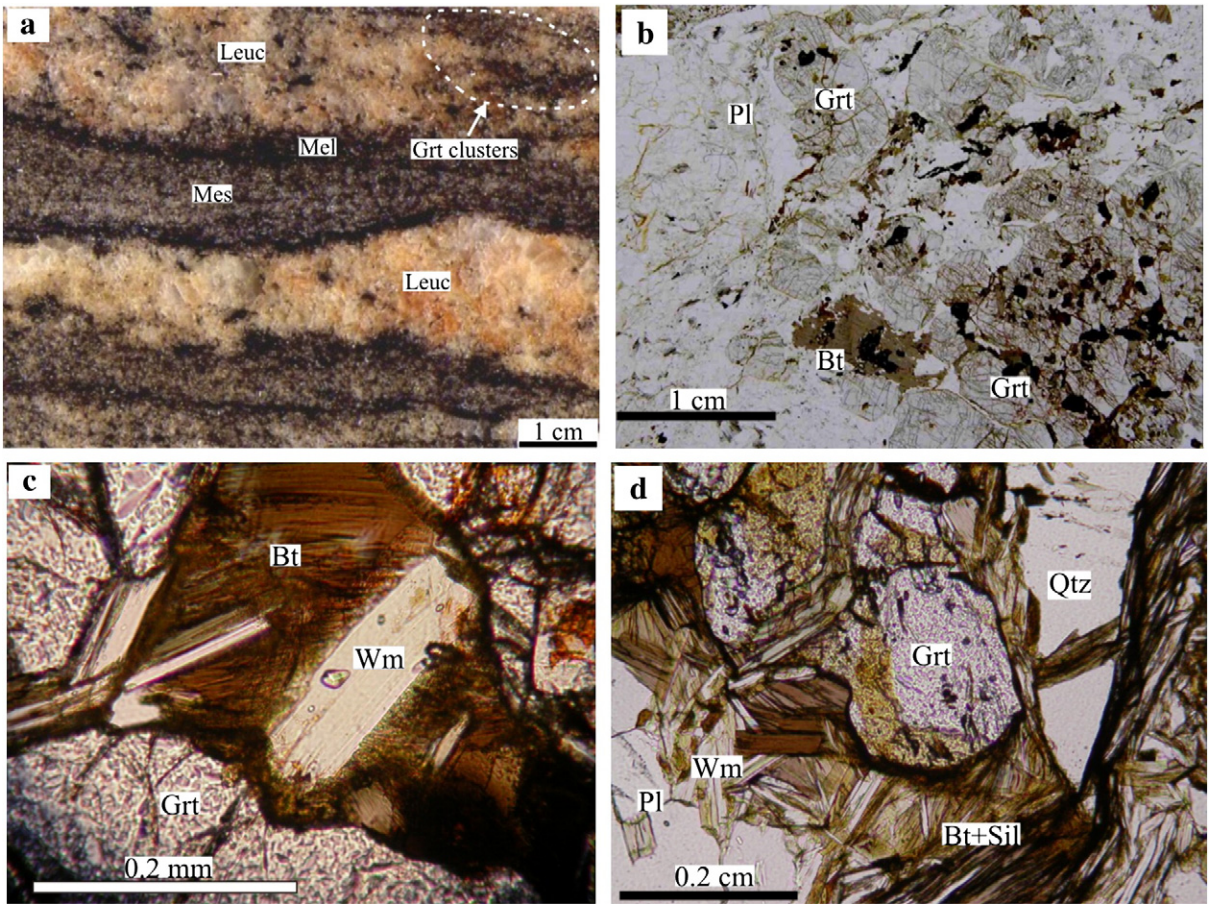

Fig. 3. (a) Compositional layering of a stromatic migmatite in the GrBPM showing well defined mesosomes, Bt-Sil rich melanosomes and leucosomes with Grt-clusters (a) and (b). (c) Biotite and white mica included in a Grt-core. (d) Equilibrium Grt–Bt–Wm–Sil–Qtz assemblage in a micaceous domain of the Pel-X.

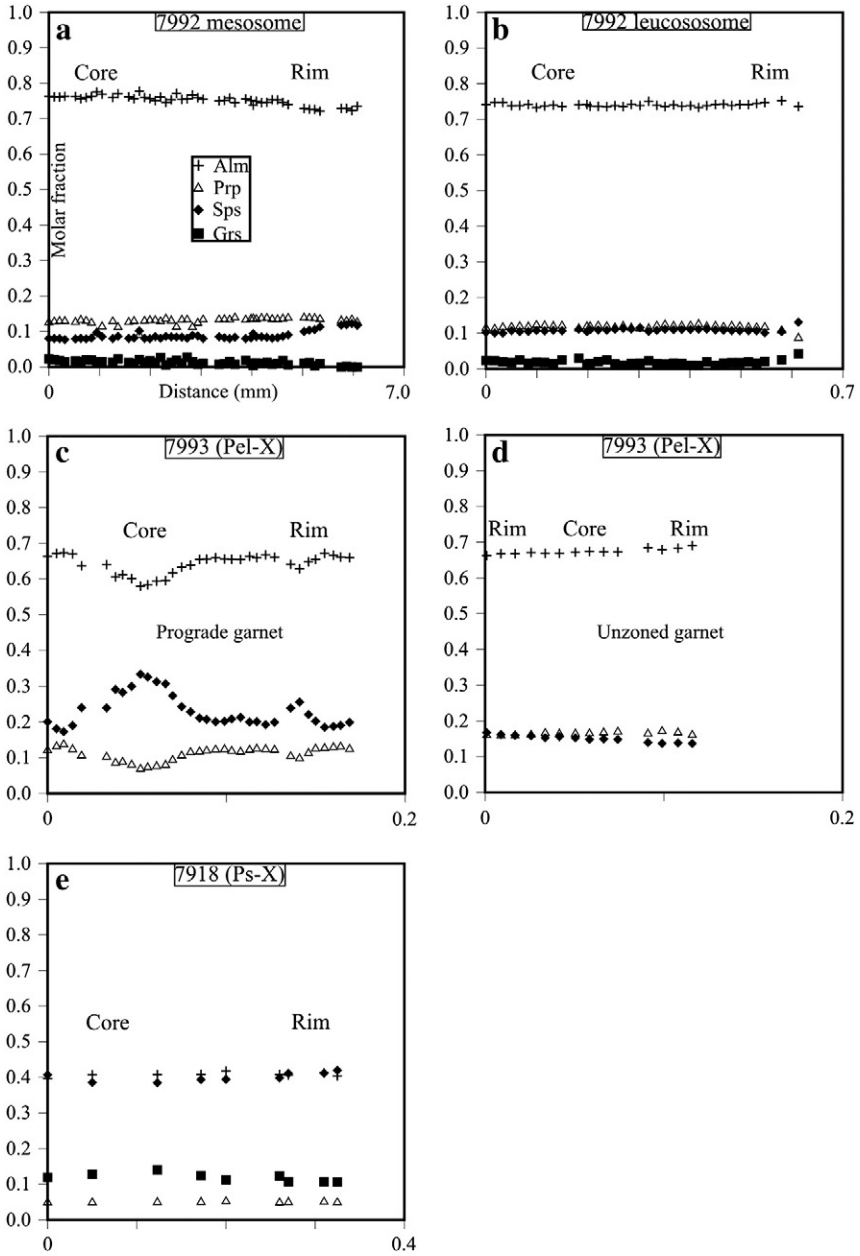

Fig. 4. Compositional garnet-end member profiles. (a) and (b) represent diffusion-driven patterns in garnet within mesosome and leusosome of the GrBPM, respectively. Both zoning patterns show retrograde increase in the Sps content toward the rims. (c) Garnet in the Pel-X showing a relic prograde inner core (high Sps content) and outer core and rims affected by diffusive cation re-equilibration. (d) Small garnet totally affected by thermal diffusion (flat zoning) and showing no retrograde equilibration. (e) Garnet in the Ps-X with diffusion-driven zoning patterns for Sps, Alm and Prp, the core preserving some of the growth-zoning for grossular (higher content). See further explanations in text.

X_{Fe} (0.58–0.60, see supplementary table in the electronic Appendix A). Neither retrograde textures nor minerals are observed. Thus, the prograde equilibrium mineral assemblage for this sample is Grt + Bt + Wmca + Pl + Qtz ± Sil. Si content in white mica is the highest among the studied samples (6.34–6.40 a.p.f.u., O = 22).

3.3. Sample 7918: metapsammite xenolith in the FPG (Ps-X)

Micas are poorly-aligned and texture is rather massive, showing sometimes incipient schistosity. The rock is medium grained, quartz rich, white mica-free, and composed of quartz, plagioclase, biotite, garnet, apatite, zircon and ilmenite.

Garnet is always poikiloblastic and normally appears as subhedral to euhedral blasts. It contains inclusions of quartz, biotite and plagioclase, suggesting textural equilibrium between these phases. It is spessartine- and grossular-rich ($Alm_{40–47}Grs_{8–14}Prp_{5–8}Sps_{34–42}$, see supplementary table in the electronic Appendix A). Profiles of chemical composition are nearly flat and exhibit incipient retrograde pattern for spessartine towards the outer rims (Fig. 4e), although retrograde minerals were not observed. Plagioclase is unzoned and andesine in composition ($An_{29–36}$, see supplementary table in the electronic Appendix A). Biotite is Al poor and X_{Fe} values are intermediate (0.50 to 0.54, see supplementary table in the electronic Appendix A). The equilibrium mineral assemblage is assumed to be Grt + Bt + Pl + Qtz.

3.4. Sample 7901: cordierite-bearing metapelitic septa in the CBG (CBMS)

Micas are roughly aligned and define a poor schistosity. Sometimes schistosity is absent and the rock shows massive texture. The rock is medium to fine grained and composed of quartz, biotite, white mica, plagioclase, cordierite, sillimanite, ilmenite, zircon and apatite. Cordierite

poikiloblasts are characterized by anhedral contours showing no or incipient pinnitization. Core and rim compositions are nearly identical and characterized by high X_{Mg} (0.65–0.66) and Na (0.08–0.10) contents. Biotite and white mica are present either as disseminated flakes or inclusions in cordierite, showing no compositional variation related to their position in the fabric (see supplementary table in the electronic Appendix A). Sillimanite is present in the prismatic and fibrous varieties, generally associated to micas and cordierite. The equilibrium contact metamorphic assemblage is Crd + Qtz + Pl + Bt + Wmca ± Sil. Si content in white mica is low (6.09–6.12 a.p.f.u., O = 22).

4. Interpretation of the petrographic observations

Sillimanite-bearing peak assemblages in the GrBPM and xenoliths of the southern region and the CBMS of the northern region indicate HT metamorphism associated to granitic intrusions. However, metasedimentary rocks of the southern region underwent partial melting and commonly contain garnet, whereas hornfels of the northern region are cordierite-bearing and garnet-absent indicating lower pressures (e.g. Miyashiro, 1994).

The GrBPM contain white mica coexisting with garnet and other minerals in leucosomes without K-feldspar. It rules out dehydration melting of metapelites at >800 °C, where white mica is totally consumed and leucosomes are characterized by K-feldspar + sillimanite + biotite (e.g. Thompson, 1982; Vielzeuf and Holloway, 1988). Leucosome formation in the GrBPM can be better explained by lower temperature hydration melting (e.g. Patiño Douce and Harris, 1998):

$$Wmca + Pl + Qtz + H_2O = melt$$

In this reaction, white mica dissolves congruently to form melt and K-feldspar, sillimanite and biotite are not formed by white mica dehydration (Patiño Douce and Harris, 1998). Garnet is interpreted to be peritectic in origin and in equilibrium with melt-crystallized minerals. One possible peritectic garnet-forming reaction is (e.g. Whitney and Irving, 1994):

$$Pl + Qtz + Bt(and/or Wmca) + Als + H_2O = melt + Grt$$

Sample 7901 (CBMS) contains the equilibrium mineral assemblage Crd + Qtz + Pl + Bt + Wmca ± Sil. Classical sillimanite- and cordierite-forming dehydration reactions at high T/P (~640 °C and <5 kbar) are (e.g. Bucher and Frey, 1994):

$$Wmca + Qtz = Kfs + Sil + H_2O \text{ and } Sil + Bt + Qtz = Crd + Kfs + H_2O$$

However, the CBMS is K-feldspar absent and white mica is observed either included in cordierite or in the matrix without compositional difference, suggesting equilibrium. A probable reaction that causes coexistence of cordierite and white mica at ~650 °C and ~2 kbar is in the form of reaction (e.g. Spear and Cheney, 1989):

$$Bt + Als + Qtz = Grt(Alm) + Crd + Wmca + H_2O$$

This reaction explains satisfactorily the Crd–Wmca coexistence although garnet is absent in the CBMS, probably due to the bulk-chemical composition.

5. Geothermobarometry

To obtain reliable P–T metamorphic and igneous emplacement conditions, several independent thermobarometrical methods, thermodynamic databases and activity models were used. Conventional thermobarometry as well as multiphase equilibria methods were matched with results from P–T pseudosections in metasedimentary rocks. For mixing models and thermodynamic databases of the used softwares, see references of each version.

We used the multiphase equilibria TWQ software (Berman, 1991) with the database of version 2.32 (DEC06.DAT, DEC06.SLN). To test the validity of the results from TWQ with independent thermodynamic databases and activity models, we used the conventional barometers garnet–biotite–muscovite–aluminosilicate–quartz (GBMAQ; Wu and Zhao, 2007) and garnet–biotite–plagioclase–quartz (GBPQ; Wu et al., 2004). The latter was applied on sample 7918 (Ps-X) which lacks of white mica and aluminosilicates. Temperatures necessary to apply both barometers were calculated by using the Grt–Bt thermometer with mixing models of Holdaway (2000), which is included in the spreadsheets of the GBMAQ and GBPQ barometers. P–T pseudosections were calculated using the PERPLE-X (version 2007) software package (e.g. Conolly, 1990). The internally consistent thermodynamic database of Holland and Powell (1998) — updated by Holland (2002) and the activity models of the corresponding version (Solut_07.dat) were used. Bulk major element compositions are shown in a supplementary table in the electronic Appendix A. For all calculations, H_2O and O_2 were assumed to be in excess. Pseudosections were useful to estimate P–T conditions from: a) Calculation of the compositional variation of solid-solution end members (e.g. isopleths); and b) reconstruction of stability fields of theoretical assemblages and comparison to observed mineral assemblages. Na-in-cordierite temperatures were calculated for the CBMS in order use them as a tool for pressure estimations in the pseudosection. The calibration of Mirwald et al. (2008) for high X_{H2O} and relatively low temperature was preferred for this thermometer, since cordierite-white mica coexistence suggests temperatures around 650 °C (see previous section).

5.1. Southern region: high temperature/medium pressure metamorphism

P–T calculations were made for mesosome and leucosome in the GrBPM. P–T results from mesosome and leucosome are very similar (see details in a supplementary table in the electronic Appendix A) and ranges described below are valid for both domains. Temperatures calculated using the garnet-biotite geothermometer yielded by the TWQ software (calibration of version 2.32) are slightly lower than those from GBMAQ thermobarometry (Grt-Bt thermometer of Holdaway, 2000). GASP pressures were not calculated for garnet cores in any case due to the lack of plagioclase inclusions. P–T calculations for garnet rims combined with biotite and white mica in the matrix yielded temperatures of 565–599 °C and pressures of 4.0–4.9 kbar (GBMAQ). P–T conditions calculated with TWQ were 550–586 °C and 3.8–5.1 kbar. Temperatures for core analysis reached slightly higher values of 580–630 °C, whereas pressures are nearly the same. These temperatures are lower than those of ~700–750 °C obtained by Patiño Douce and Harris (1998) for hydration partial melting of a micaceous schist at medium pressure and could not reflect peak conditions. Thus, a pseudosection to predict partial melting excluding K-feldspar end-members was calculated for the bulk composition of an unmolten micaceous gneiss (sample 7992gn) closely associated to the GrBPM (Fig. 5a). This gneiss is thought to well represent the migmatite protolith, since its mineral assemblage Grt + Bt + Wmca Pl + Sil and Kfs-absent is similar to the GrBPM. The pseudosection predicts that leucosome (melt-in curve) coexisting with Bt–Wmca–Pl–Grt–Sil–Qtz appears at around 780 °C and ~5 kbar. It is also predicted that cooling should occur without important changes in pressure, because if pressure falls suddenly cordierite (absent in the studied migmatites) should form region of the leucosome mineral assemblage.

The same thermometers and barometers as for the GrBPM were applied in the Pel-X (sample 7993). Due to virtually absent grossular contents, the GASP barometer was not used. Garnet chosen for conventional calculations were small unzoned grains, considered to yield peak conditions since they are totally surrounded by micas. Results

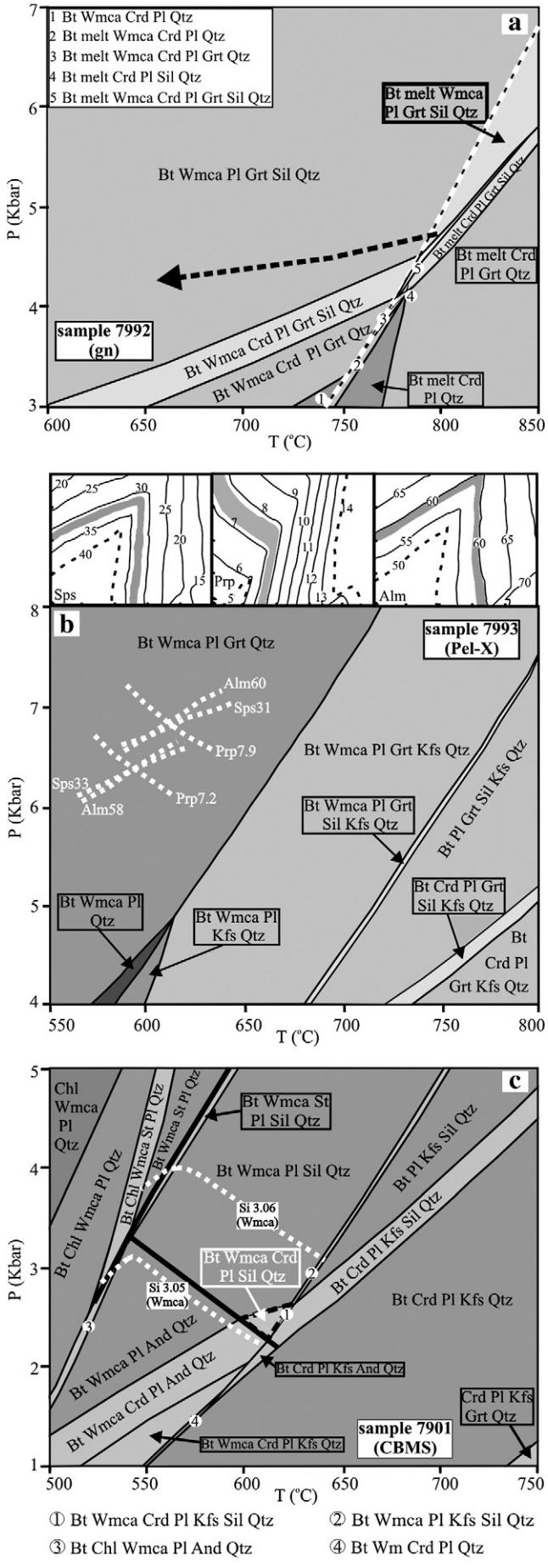

are listed in a supplementary table in the electronic Appendix A. Calculated temperatures from TWQ and GBMAQ are 691–766 °C and 668–762 °C, respectively. GBMAQ pressures were calculated in 5.8–7.0 kbar. To obtain initial conditions of the metamorphism, isopleths for end member core compositions of prograde garnet (Fig. 4c) were plotted in a P–T pseudosection (Fig. 5b). Spessartine, almandine and pyrope-isopleths intersect at one point for inner core compositions and define a small area for the outer core. Both intersections yield a good estimation at about 580–610 °C and 6.3–6.7 kbar.

Conventional Grt-Bt temperatures from the Ps-X (sample 7918) are ~50 °C higher than those from TWQ (612–651 °C and 558–598 °C, respectively). Pressures using the GASP (TWQ) and GBPQ barometers are in acceptable agreement, ranging from 5.4 to 6.8 kbar and from 5.8 to 7.1 kbar respectively (see Supplementary Table in the electronic Appendix A). GASP pressures are assumed to be maximal, since sillimanite is not present in the sample.

5.2. Northern region: high temperature/low pressure metamorphism

Pressure-independent temperature estimates were made by using the Na-in-cordierite thermometer in the CBMS (sample 7901). Temperatures range from 604 to 654 °C (details in a supplementary table in the electronic Appendix A). The absence of suitable minerals for pressure calculations led to the modelling of a pseudosection to better constrain metamorphic conditions (Fig. 5c). A small-sized and low-variance stability field was obtained for the calculated assemblage Bt–Wmca–Crd–Pl–Sil–Qtz, which is in exact agreement with the observed one. The stability field is within the range of 600–645 °C and 2.2–2.6 kbar. Temperatures are in good agreement with those from Na-in-cordierite. Si-isopleths for white mica were plotted in the pseudosection since Si content in white mica is strongly pressure-dependent (e.g. Massonne and Schreyer, 1987). The field between both extreme Si contents of white mica in sample 7901 (3.05–3.06 for O = 11) encloses the stability field for the mineral assemblage. The latter gives thus a good estimate of the contact metamorphic P–T conditions.

6. Geochronology

6.1. Granitic rocks

U–Pb conventional (ID-TIMS) zircon and monazite dating was carried out on three samples corresponding to three Ordovician granitic bodies of the study area (FPG, BPG and CBG) and two Carboniferous ones. Isotopic U–Th–Pb analysis and age calculations are listed in Table 1. Analytical methods are described in the electronic Appendix A. The high zircon content in sample 7920 (BPG) was sufficient to collect three different batches of grains, whereas zircon grains from the other samples had to be abandoned due to their scarcity and/or poor quality. Most of the monazite ages are slightly reversely discordant. Reverse discordance in monazite may be owed to an excess in ^{206}Pb due to the decay of ^{230}Th (Schärer, 1984). Since monazite contains high Th content, there is a significant percentage of short-life ^{230}Th which is an intermediate product in the decay chain of ^{238}U to ^{206}Pb. ^{230}Th subsequently decays to ^{206}Pb and is incorporated in significant amounts

Fig. 5. P–T pseudosections in the CNKMnFMASH system of representative metasedimentary rocks. Stability field are darker as the variance increases. Bold letters in (a) and (c) are predicted assemblages which agree with observed assemblages. (a) The "melt" component was incorporated to predict the generation of partial melts in the GrBPM. The white dashed line represents the melt-in curve. The bold dashed arrow indicates the inferred P–T path. (b) Prograde metamorphic conditions of the Pel-X modelled from Grt end member-isopleths for core compositions. Isopleths for each end member are plotted on the top of the pseudosection; shaded fields are areas between maximal and minimal values. Isopleth-intersections are represented by white bold lines in the pseudosection. (c) P–T contact metamorphic conditions of the northern region of the block (CBG + CBMS) well constrained by a small stability field for the assemblage Bt–Wm–Crd–Pl–Sil–Qtz. Part of the Si-isopleths for maximal and minimal content in the sample in white mica are plotted with white lines.

Table 1
U–Pb analytical data for monazite and zircon. Granitoids.

Sample	Wt (μg)	Pb (ppm)	U (ppm)	$^{206}Pb/^{204}Pb$ meas.	Calculated isotopic ratios						Ages (Ma)					
					$^{206}Pb/^{238}U$[#]	2σ (%)	$^{207}Pb/^{235}U$[#]	2σ (%)	$^{207}Pb/^{206}Pb$[#]	2σ (%)	$^{206}Pb/^{238}U$	2σ	$^{207}Pb/^{235}U$	2σ	$^{207}Pb/^{206}Pb$	2σ
Monazite																
Felsic porphyritic granitoids (FPG)																
7833A(1)	3.73	123.1	1365	1255	0.07519	0.51	0.57779	0.58	0.05574	0.27	467	2.4	463	2.7	442	6.1
7833B(1)	3.73	861	1622	821	0.07684	0.50	0.59240	0.55	0.05591	0.21	477	2.4	472	2.6	449	4.7
7833C(1)	3.73	1043	2029	1733	0.07665	0.49	0.59029	0.55	0.05585	0.25	476	2.3	471	2.6	446	5.6
7833D(1)	2.01	252.3	445	979	0.07647	0.74	0.60093	1.69	0.05700	1.52	475	3.5	478	8.1	491	34.5
7833E(1)	1.17	207.5	446	430	0.07720	1.89	0.59912	2.13	0.05628	0.95	479	9.1	477	10.2	464	21.5
Average ages (grain 7833A excluded)											**476.4**	**1.5**	475.8	2.2	449	16
Biotitic porphyritic granitoids (BPG)																
7920(1)	3.7	212.3	1092	3257	0.07411	0.47	0.56881	0.49	0.05566	0.11	461	2.2	457	2.2	439	2.5
Cordierite-bearing granitoids (CBG)																
7903A(1)	2.07	221.9	1301	1472	0.07581	0.64	0.59047	0.75	0.05649	0.39	471	3.0	471	3.5	472	8.8
7903B(1)	1.17	128.4	1849	1932	0.07246	0.61	0.56122	0.71	0.05617	0.37	451	2.8	452	3.2	459	10.4
7903C(1)	1.9	166.7	1015	1388	0.07622	0.56	0.58359	0.73	0.05553	0.46	474	2.7	467	3.4	434	10.3
Average ages (all grains included)											**465**	**12**	459	150	456	26
Undeformed granular monzogranite (Huaco Pluton)																
7592A(1)	7.74	169.6	291	629	0.06	0.83	0.41	0.95	0.05	0.46	360	3.0	348	3.3	267	8.2
7592B(1)	1.1	386.6	1385	547	0.06	1.14	0.42	1.21	0.05	0.40	360	4.1	359	4.3	353	8.3
7592C(1)	4.66	236.4	638	1878	0.06	0.53	0.42060	0.56	0.05300	0.18	361	1.9	356	2.0	329	3.6
Average ages (all grains included)											**360.4**	**2.9**	360.8	2.4	319	82
Undeformed porphyritic granite (Sanagasta Pluton)																
7826(1)	4.78	180.9	268.9	376	0.05759	2.03	0.41700	2.23	0.05251	0.88	361	7.3	354	7.9	308	17.1
7826(1)	4.64	217.9	456.9	1193	0.05751	0.78	0.42144	0.85	0.05315	0.33	360	2.8	357	3.0	335	6.7
7826(1)	1.87	422.9	633.0	749	0.06	1.18	0.42	1.31	0.05	0.56	361	4.3	356	4.7	319	11.1
7826(1)	2.99	356.4	615.8	319	0.06	0.94	0.42	1.01	0.05	0.34	360	3.4	355	3.6	322	6.8
7826(1)	4.78	49.5	341.4	346	0.06	1.03	0.42	1.16	0.05	0.53	362	3.7	357	4.1	326	10.6
Average ages (all grains included)											**360.6**	**3.7**	360	7.1	326	13
Zircon																
Biotitic porphyritic granitoids (BPG)																
7920A(7)	42.8	11.8	153	664	0.07456	1.26	0.56724	2.73	0.05518	2.42	464	5.8	456	12.4	419	53.6
7920B(19)	35.4	27.8	363	681	0.07375	0.51	0.58482	0.59	0.05752	0.29	459	2.3	468	2.8	511	6.6
7920C(20)	20	45.1	496	247	0.07435	0.50	0.58252	0.54	0.05682	0.20	462	2.3	466	2.5	485	4.5
Average ages (all grains included)											**461**	**11**	463.2	2.7	492	18

U and Pb concentrations corrected for blank.
Blank corrections: standards NBS 982 (Pb) and U500 (U) were used for measurement control.
Ages calculated using the Isoplot/Ex 3.0 software of Ludwig (2003).
Decay constants recommended by the IUGS (Steiger and Jäeger, 1977).
7920r(7): Sample (number of grains).
Selected average ages are in bold.
[#] Radiogenic Pb corrected for blank and initial Pb. U corrected for blank.

in the crystal during crystallization of monazite, causing a ^{206}Pb excess and thus reverse discordance (Schärer, 1984; Parrish, 1990; Foster et al., 2000). However, it is evident that in our case this effect is very small and causes slight discordance. $^{207}U/^{235}Pb$ ages should be closer since they are not affected by the thorogenic ^{206}Pb excess although they are less precise from an analytical point of view due to the low ^{207}Pb contents. From the above exposed, we consider the $^{206}Pb/^{238}U$ ages to be the closest estimates for the age of monazite.

Sample 7833 (FPG) is represented by a two-mica porphyritic shear-deformed monzogranite with low proportion of micas and moderate post-magmatic foliation, collected near the contact with the BPG. Four single-grain monazite analyses of this sample yielded an average $^{206}Pb/^{238}U$ age of 476.4 ± 1.5 Ma (Fig. 6a).

Sample 7920 (BPG) represents a porphyritic biotitic granodiorite with weak to absent shear deformation, collected a few kilometers eastward from the contact with the FPG. The only single-grain monazite analysis of this sample yielded a younger $^{206}Pb/^{238}U$ age of 461 ± 2.2 Ma (Fig. 6b) respect to the FPG. In addition, three multi-grain zircon fractions from the same sample (7920) plotted close to the concordia curve and yielded an average $^{206}Pb/^{238}U$ age of 461 ± 11 Ma, overlapping with the $^{206}Pb/^{238}U$ monazite age (Fig. 6b).

Sample 7903 (CBG) is a granular monzogranite with abundant cordierite (up to 10 vol.%), collected at the contact with the LCF. A $^{206}Pb/^{238}U$ age of 465 ± 12 Ma was obtained for the CBG from three monazites, which overlaps with the other ages due to its large 2σ error (Fig. 6c).

Additionally, two undeformed younger granitoids in clear intrusive relationship with the Ordovician ones were dated to improve geochronological constraints in the study area. Sample 7592 is a granular cordierite-absent two-mica monzogranite that intruded the CBG and the LCF in the northern region of the study area. A $^{206}Pb/^{238}U$ age of 360.4 ± 2.9 Ma was obtained from three monazite grains within this sample (Fig. 6d). Sample 7826 represents a strongly porphyritic two-mica syenogranite collected in the southern region near the contact with the FPG. A similar $^{206}Pb/^{238}U$ age of 360.6 ± 3.7 Ma was obtained from five monazite grains within this sample (Fig. 6e).

6.2. GrBPM

Pb, Th and U contents in monazite grains included in garnet within two polished sections representing the two domains of the GrBPM (7992mes and 7992leu) were analyzed *in situ* using an electron microprobe. Analytical methods are described in the electronic Appendix A. Normalization of the elements was calculated to eight valences. For age determinations, the 1σ standard deviations were calculated by error propagation of the analytical uncertainties of the single elements based on Poisson statistics. These 1 σ values range from 7.4 to 10.5 Ma for monazites in the leucosome and from 9.4 to 10.1 Ma for those in the mesosome. Ages for single grains were calculated according to Scherrer et al. (2000). Five grains and fifteen grains were analyzed in mesosome and leucosome respectively

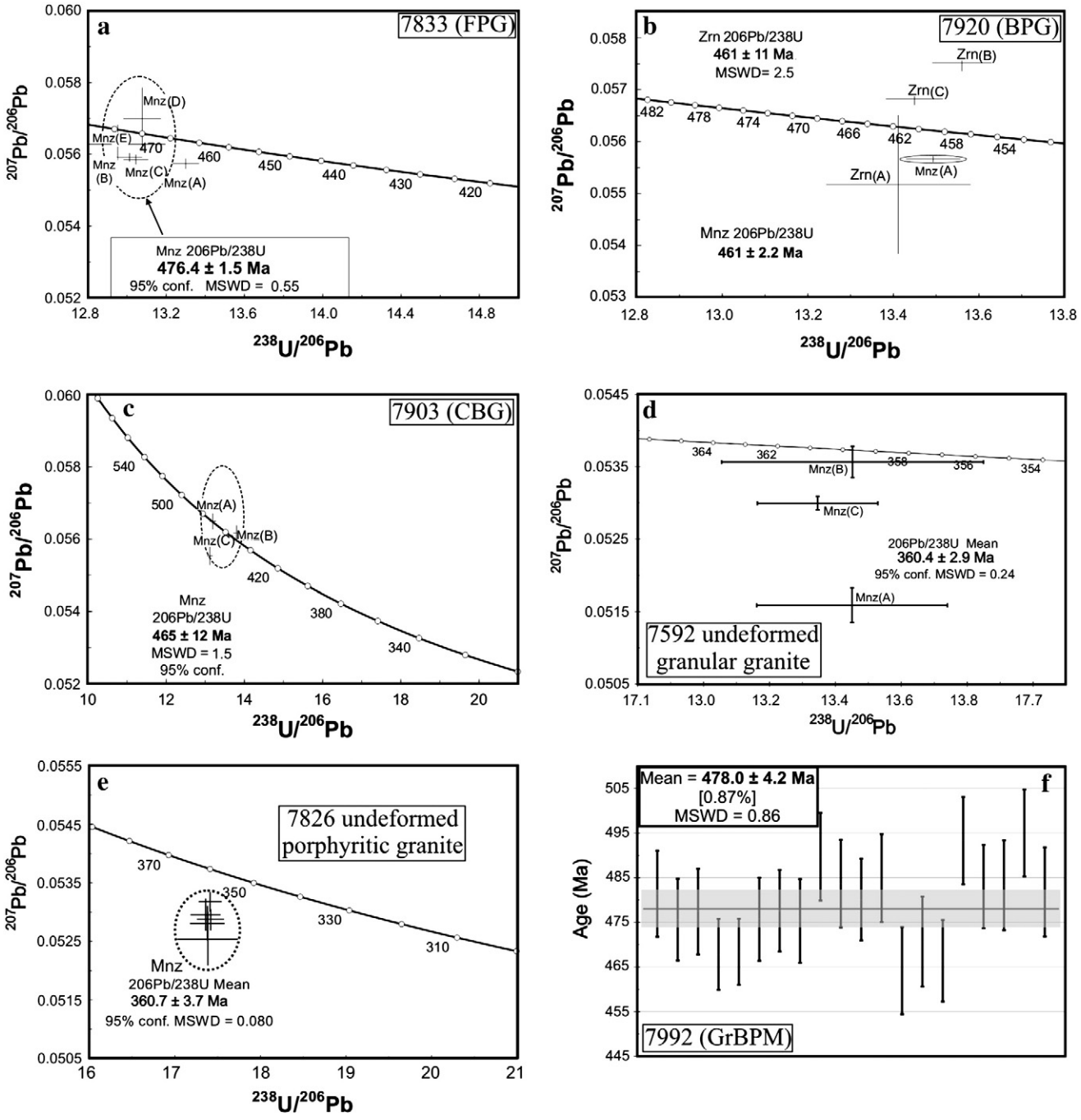

Fig. 6. (a–e) U–Pb monazite and zircon isotopic analyses plotted in Tera–Wasserburg diagrams. Data-point error crosses are 2σ. Mean ages are indicated in bold. U–Pb ages in zircon were calculated for the BPG as there are only zircon data for the BPG (b). (f) U–Th–Pb Weighted average monazite ages calculated from *in situ* single-grain EMP analysis. Data-point error bars are 2σ. Error percentages are in brackets.

(Table 2 and also see a Supplementary Table in the electronic Appendix A). We found no statistically significant difference in mean ages from both domains. The calculated weighted average age for twenty monazite grains in the mesosome and leucosome is 478 ± 4.2 (Fig. 6f).

7. Interpretation of the age results

Coupling growth of garnet with monazite frequently occurs over a wide interval from sub-solidus to peak metamorphic conditions, since high rates of monazite-forming elements occur as garnet grows (e.g. Rubatto et al., 2006; Gaidies et al., 2008). It makes monazite a potential tool to date metamorphic events. Thus, we assume that garnet and monazite inclusions grew together during migmatization and they constitute a good approach to the age of the peak metamorphism. On the other hand, monazite ages for the FPG and the leucosome of the GrBPM are in good agreement (~478 and 475 Ma respectively). It suggests that incipient anatexis of the GrBPM and granitoid intrusion were coeval and occurred at similar crustal levels (~14–18 km), supporting field observations at the intrusive contact. The timing of intrusion of the BPG and CBG could not be discerned, since 2σ errors give place to large uncertainties of around 20 Ma and ages overlap. However, from field relationships and thermobarometry it can be inferred that the CBG is the youngest pluton, since it intruded the older mid-crustal FPG when it had reached the upper crust by exhumation. U–Pb ages obtained in this work agree within errors with

Table 2
1σ errors for Y, Th, U and Pb and calculated single grain ages for the GrBPM.

Sample	σY	σTh	σU	σPb	Age (Ma)	1σ (Ma)
7992mes	0.0175	0.0172	0.0059	0.0023	493.3	9.8
7992mes	0.0198	0.0176	0.0060	0.0023	483.0	9.3
7992mes	0.0194	0.0174	0.0057	0.0023	483.3	10.1
7992mes	0.0249	0.0176	0.0058	0.0023	495.0	9.7
7992mes	0.0225	0.0171	0.0058	0.0023	481.8	10.0
7992leu	0.0197	0.0171	0.0060	0.0023	481.4	9.6
7992leu	0.0219	0.0181	0.0059	0.0023	475.6	9.1
7992leu	0.0176	0.0166	0.0061	0.0023	477.4	9.6
7992leu	0.0129	0.0205	0.0059	0.0024	467.8	7.9
7992leu	0.0147	0.0203	0.0063	0.0024	468.4	7.4
7992leu	0.0164	0.0173	0.0060	0.0023	475.7	9.3
7992leu	0.0217	0.0181	0.0059	0.0023	477.6	9.1
7992leu	0.0149	0.0174	0.0059	0.0023	475.3	9.4
7992leu	0.0216	0.0176	0.0057	0.0023	489.7	9.8
7992leu	0.0219	0.0176	0.0058	0.0023	483.7	9.8
7992leu	0.0208	0.0180	0.0059	0.0023	480.1	9.2
7992leu	0.0205	0.0173	0.0058	0.0023	484.9	9.8
7992leu	0.0206	0.0172	0.0058	0.0023	464.2	9.8
7992leu	0.0198	0.0178	0.0056	0.0023	470.7	10.1
7992leu	0.0177	0.0172	0.0061	0.0023	466.4	9.1
Weighted mean age: 478.0 ± 4.2 Ma						

Note: The age was calculated according to Scherrer et al. (2000). Errors for weighted mean ages were calculated to 2σ.

those recently obtained in the Sierra de Velasco and neighbour regions and confirm that the Ordovician magmatism of the Famatinian belt lasted around 20–30 Ma (e.g. Pankhurst et al., 2000; Dahlquist et al., 2008). The Devonian/Carboniferous ages of samples 7592 and 7826 are similar to previously obtained U–Pb ages for the Huaco and Sanagasta plutons (Grosse et al., 2009). The granular granite of sample 7592 can be interpreted as a chilled margin of the Huaco Pluton, whereas the strongly porphyritic granite of sample 7826 seems to be spatially related to the Sanagasta Pluton.

8. Discussion

8.1. P–T paths: metamorphic evolution

P–T paths derived for some of the samples permitted us to distinguish three different crustal levels of the metasedimentary basement (Fig. 7). We consider that the xenoliths included in the FPG and BPG were carried from a level I at ~20–25 km depth (5.8–7.1 kbar), assuming an average density of 2800 kg/m^3. Migmatization of the GrBPM and intrusion of the FPG and BPG occurred in a shallower level II at ~14–18 km depth (4.0–5.1 kbar). Intrusion of the CBG and metamorphism of the CBMS occurred later in the shallowest level III at ~8–10 km. Levels I and II evolved earlier in the middle crust and level III characterizes the Paleozoic upper crust of the study area and neighbour regions. The deeper level I underwent prograde isobaric heating from ~580 to 750 °C that was recorded in the Pel-X. Relatively high pressures of level I are confirmed by the Ps-X contained in the FPG. Temperatures of ~600 °C from thermobarometry for the GrBPM are considered to represent part of the cooling history of level II. The thermal peak for the migmatization occurred earlier at ~780 °C and similar depths. Thus, level II is characterized by isobaric cooling of around 200 °C. The HT/LP metamorphism of level III superimposed on level II when the latter was exhumed to the upper crust. It is striking that the highest temperatures reached during the prograde history of level I are lower than those of the

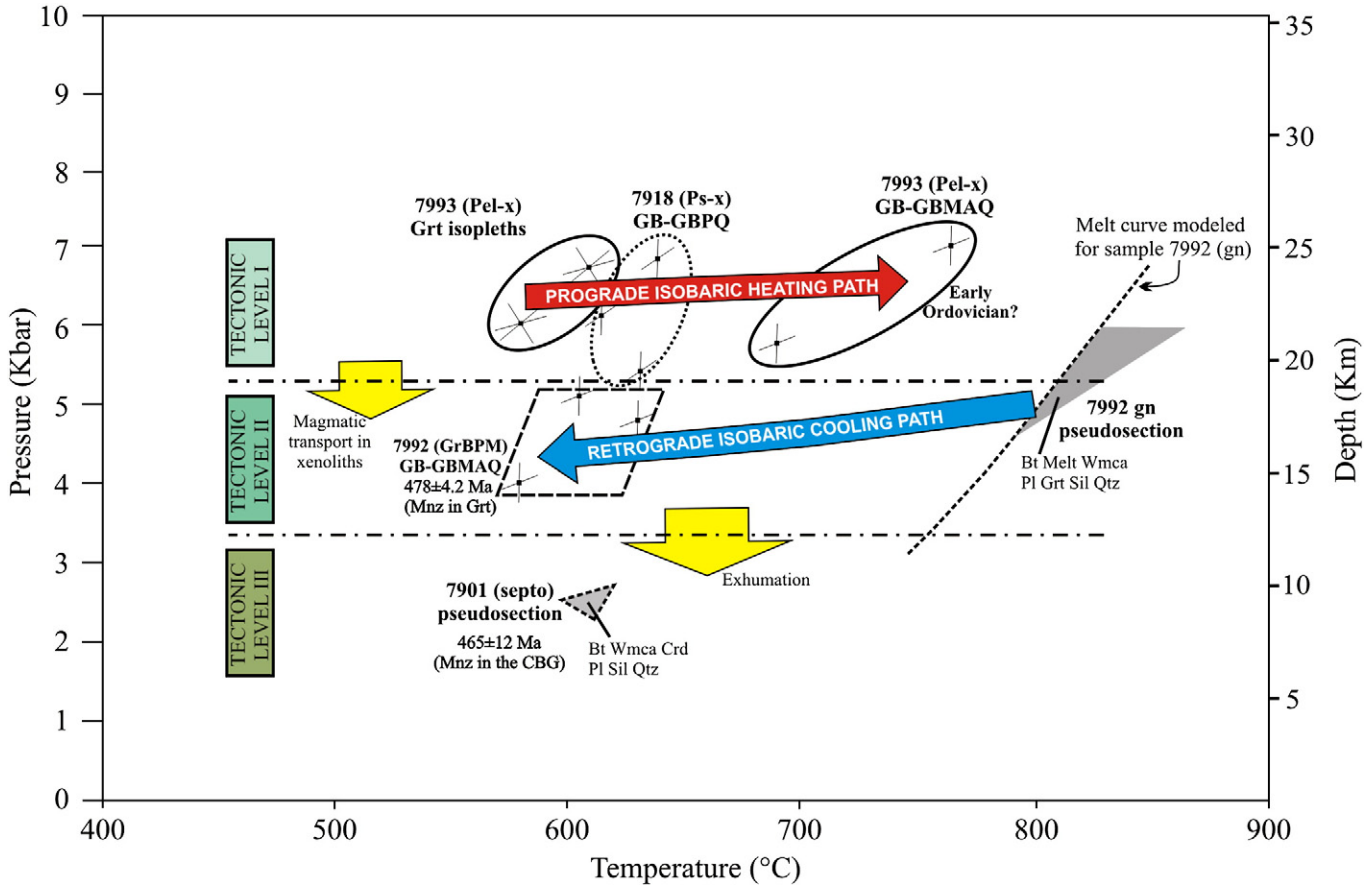

Fig. 7. Ordovician metamorphic P–T paths from thermobarometry on the studied rocks. Prograde metamorphism was recorded in xenoliths and occurred in the deepest tectonic level I. Xenoliths of level III were carried upwards by the FPG and the BPG, which intruded in level II. The intermediate level II is characterized by isobaric cooling of the GrBPM. Level III is a supracrustal level in which the CBG intruded and caused localized HT/LP metamorphism in the La Cébila Formation. Level III is the earlier mid-crustal level II exhumed to the upper crust. Level III remained in the upper crust until the intrusion of Early Carboniferous plutons.

thermal peak of level II, which implies that a "colder" level underlies a "hotter" one. A plausible explanation is that level II was originally located deeper (and hotter) than level I. Subsequently, Ordovician inverse shear movements may have thrusted level I under level II. Hence level II cooled isobarically from high (~800 °C) temperatures whereas level I evolved through isobaric heating at deeper levels. This mechanism requires fast shear movement compared to rates of metamorphism. Evidence of crustal stacking by Ordovician HT reverse ductile shear zones has been observed in the migmatitic basement of the Famatinian Belt (Willner et al., 1987).

8.2. P–t paths: exhumation rates

Since pressure relates directly with depth and time lapses can be assumed from geochronology, P–t information is one of the best tools to estimate exhumation rates (Ring et al., 1999). In our study, estimates in depth of metamorphism are acceptably constrained, whereas uncertainties in age lead to wide-ranging estimates of exhumation rates (Fig. 8). No exhumation can be resolved for level I, since it is represented by xenoliths transported by granitic plutons and the timing of prograde metamorphism is unknown. Isobaric cooling of the GrBPM allows using the well-constrained peak metamorphic age of 478 ± 4 Ma as associated to the depths of 14–18 km for level II. The timing of contact metamorphism of level III (8–10 km depth) is represented by the poorly-constrained age of 465 ± 12 Ma of the CBG. Consequently, Ordovician exhumation from level II to level III must be resolved by assuming minimal and maximal lapses of time. The minimal lapse can be assumed from the central values of ages (478 Ma and 465 Ma), which translates to a maximal integrated mean exhumation rate of 0.38–0.78 mm/yr. The maximal lapse is assumed from 2σ errors which are in the order of ~20 Myr and correlate with the maximal span for the Ordovician magmatism of the region (e.g. Dahlquist et al., 2008). It yields minimal mean Ordovician exhumation rates of 0.25–0.51 mm/yr, consistent with the above range.

The supracrustal level III was intruded by the Devonian/Carboniferous Huaco and Sanagasta plutons at slightly shallower levels in the upper crust. Alasino et al. (2009) used the igneous assemblage Grt + Bt + Pl + Qtz ± Ms to calculate accurate emplacement pressures of 1.8–1.9 ± 0.1 kbar on Carboniferous granites of the northern region of the Sierra de Velasco. These values are consistent with field evidence of Carboniferous plutons causing brittle deformation of the host-rock during intrusion in nearby areas (e.g. Báez et al., 2005; Alasino, *pers. comm.*). We thus take calculations of Alasino et al. (2009) as the closest estimate for pressure emplacement of the Huaco and Sanagasta plutons. In the northern region of our study area, a time-lapse of 90–100 Myr is assumed from the wide-ranging age of the CBG and the well-constrained age of margin of the Huaco Pluton (~360 Ma). The wide time-lapse and the slightly shallower emplacement of the Huaco Pluton respect to the CBG translate to very low values for mean exhumation rates of 0.01–0.03 mm/yr. A rougher calculation in the southern region of the study area allows establishing maximal limits to Ordovician–Carboniferous exhumation rates. A time-lapse of ~120 Myr is assumed from the well-constrained ages for migmatization of the GrBPM and intrusion of the FPG (476–478 Ma) and the age of ~360 Ma obtained for the margin of the Sanagasta Pluton. Mean maximal exhumation rates of 0.06–0.09 mm/yr were estimated.

Despite all our calculations are wide-ranging, it is clear that Ordovician exhumation rates are an order of magnitude faster than those from the Middle/Late Ordovician to the Lower Carboniferous. Thus, we define two exhumation periods: (a) an early period I characterized by moderate exhumations rates in the order of 10^{-1} mm/yr and (b) a latter period II with slow rates in the order of 10^{-2} mm/yr.

It must be noted that an area of at least ~500 × 250 km of the Famatinian Belt was intruded by supra-crustal granitoids in Devonian/Carboniferous times (see Fig. 1a). It means that this wide crustal segment was homogeneously exhumed to the upper crust at the end of the Famatinian orogeny. Furthermore this segment resided within the crust during more than 100 Myr indicating steady exhumation of the whole Famatinian main-arc and back-arc in the Upper Paleozoic. We hence suggest that exhumation rates of this work occurred at regional scale.

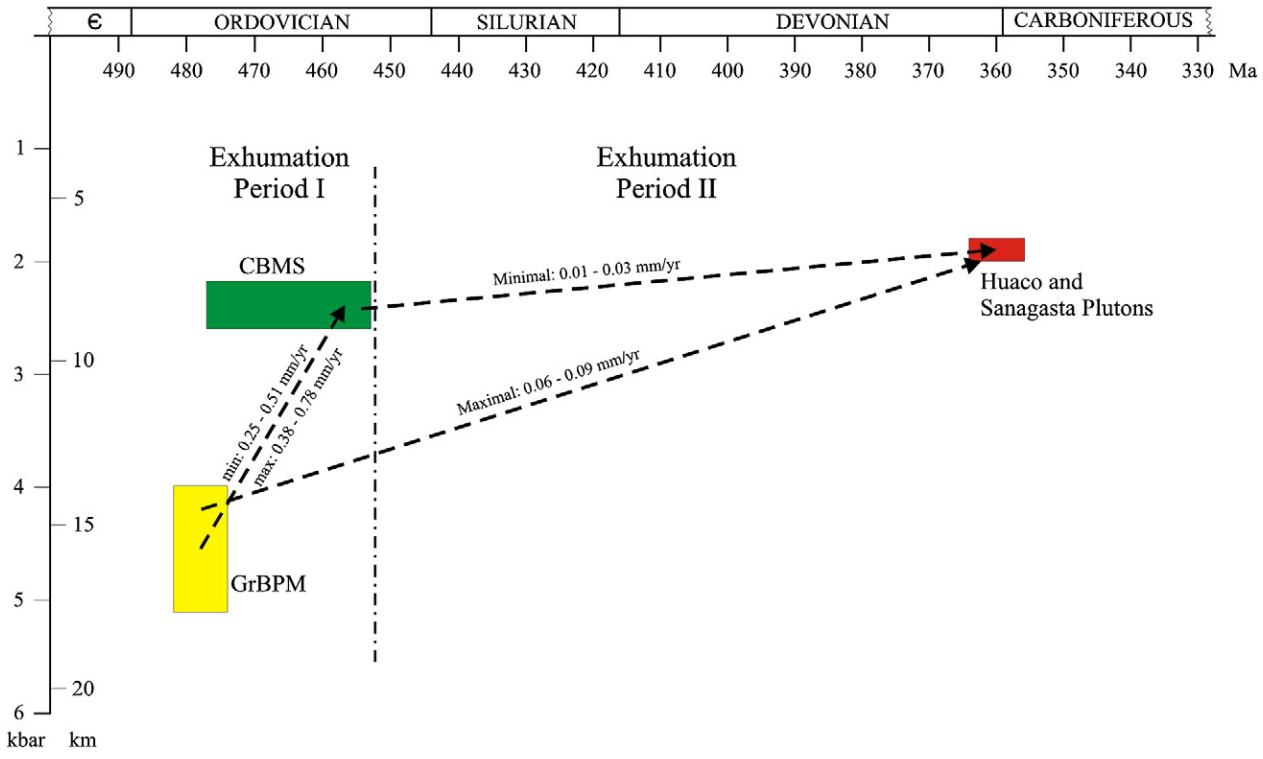

Fig. 8. Exhumation history of igneous and metamorphic rocks of the study area between the Ordovician and the Early Carboniferous. Exhumation Period I (0.25–0.78 mm/yr) occurred between the Early and Middle-Late Ordovician. The slower Exhumation Period II (0.01–0.09) occurred between the Middle-Late Ordovician and the Early Carboniferous.

8.3. Possible exhumation mechanisms

It has been proven that erosion is a primary exhumation mechanism in convergent orogens and accretionary prisms (Ring et al., 1999; Ehlers, 2005; Willner et al., 2005). Despite this mechanism can operate locally as fast as 10 mm/yr, erosion rates >0.5 mm/yr are present in only 2% of the drained area of the continents (Ring et al., 1999) and mean worldwide rates can be as slow as 0.05 mm/yr (Milliman and Syvitski, 1992). Thus, the Paleozoic exhumation rates of this work are comparable to fairly slow present-day erosion rates. However, exhumation rates alone cannot distinguish between exhumation processes. Ductile crustal thinning has been shown to be an exhumation process that also operates at rates as slow as our period II and the presence of a subhorizontal transposed foliation is diagnostic of this tectonic mechanism (Ring et al., 1999). Ductile normal faulting is an effective tectonic mechanism of exhumation that can operate at exhumation rates as fast as 3.5 mm/yr in convergent orogens (e.g. Reddy et al., 1999) although rates in the order of our period I have been reported in convergent orogens (Ring et al., 1999). Both ductile thinning and normal faulting are associated to extensional tectonics and crustal thinning, and have been interpreted to exhume granulite-facies rocks northward (the Sierra de Quilmes Metamorphic Complex, Büttner et al., 2005; Büttner, 2009) and southward (the Calamuchita Complex, Otamendi et al., 2004) of the latitude of the Sierra de Velasco. In the Sierra de Quilmes, Büttner (2009) calculated ~25–44% crustal thinning associated with extensional shearing coeval with deposition of about 7000 m marine sediments. However, extensional tectonics and thinning show the following inconsistencies when applied southwards (Sierras de Velasco, Aconquija–Ambato–Ancasti):

- The present-day crustal thickness at the latitude of the study area and adjacent regions is around 40 km (e.g. Gilbert et al., 2006). Paleodepths of ~20–25 km of the Famatinian HT/MP middle crust are widely exposed in NW-Argentina (e.g. Sierras de Ambato–Ancasti and nearby regions, Larrovere et al., 2011; Sierra de Quilmes, Büttner et al., 2005; Sierra de Velasco, this work), indicating that an equivalent overlying thickness was removed. Assuming that no significant crustal thickening occurred in the Sierras Pampeanas during the Andean orogeny, the Famatinian crustal thickness should have reached at least 60 km.
- σ- or δ-clasts and SC-fabrics as well as drag folds throughout the migmatitic basement indicate compressive W-directed ductile shearing (Willner et al., 1987; Larrovere et al., 2008), strongly suggesting crustal imbrication during thickening.
- Thick Ordovician sedimentary sequences are not present at the latitude of the Sierra de Velasco. The best known Lower Paleozoic sequence is the Volvancito Formation (Sierra de Famatina) whose thickness is less than ~500 m and was recently re-interpreted to be Upper Cambrian/Lower Ordovician in age (Tortello and Esteban, 2007).
- Nd–Sr isotopic signatures in metamorphic and igneous Famatinian rocks indicate long-lived crustal recycling and progressive homogenization during Lower Paleozoic high-T metamorphism and magmatism (e.g. Pankhurst et al., 1998, 2000).

Thus, evidence for Lower Paleozoic extensional tectonics such as either subhorizontal transposition foliation (ductile thinning) or ductile extensional shear belts (normal faulting) appear not to be present at the latitude of our study area or it is spatially subordinated. These observations stress the importance of erosion as the main exhumation mechanism of the thickened Famatinian crust in Paleozoic times and suggest that tectonic exhumation was local and/or subordinated.

8.4. Geodynamic implications

From the above exposed, we agree with the hypothesis of the Famatinian Belt as representing an ancient analogue of the Cenozoic Altiplano–Puna plateau (Lucassen and Franz, 2005). The main criteria for the Altiplano–Puna plateau development were summarized as follows (see Barnes and Ehlers, 2009 and references therein): (a) a thickened (~60–80 km) and isostatically compensated crust, (b) thin lithosphere (~100–150 km) sitting above a hot asthenospheric wedge, (c) consequent high heat flux and partial melting, thermal weakening and continuous compressive deformation of the crust and (d) piecemeal lithospheric delamination. Although we cannot unequivocally prove that all the main plateau-forming criteria are present in the Famatinian Belt, some of them are present. Willner et al. (1987) interpreted the deformation evolution of the Famatinian Belt similar to that proposed by Isacks (1988) for the Cenozoic plateau. The former workers recognized a deformation evolution characterized by a first stage of pure shear characterized by tight folding of the metasedimentary basement followed by simple reverse ductile shearing, both processes contributing to strong crustal thickening. High-T deformation of the migmatitic basement requires thermal weakening of the crust related to a thin lithosphere (~100 km), which caused shallow asthenosphere convection and high heat input (Larrovere et al., 2011). Lithospheric delamination of the Famatinian Belt is not discussed in this work although it may be related to significantly less negative εNd signatures in Devonian/Carboniferous plutons and Early/Middle Carboniferous rhyolites respect to Ordovician plutons, indicating an increase of mantle contribution in the Late Paleozoic (Grosse et al., 2009; Martina et al., 2010). Thus, we interpret that mountain-building processes similar to those which formed the Altiplano–Puna plateau may have built the Famatinian Belt in the region of our study area and we propose a schematic model (Fig. 9). Strong shortening and thickening may have occurred at the end of the previous Pampean orogeny and at starting the Famatinian orogeny (Willner et al., 1987; Whitmeyer and Simpson, 2004), accompanied by the intrusion of mid-crustal plutons in Early/Middle Ordovician times (Fig. 9a). As inferred by Schurr et al. (2006) for the Altiplano–Puna Plateau, lithospheric thinning of the Famatinian main arc and back arc was probably a result of convective removal of the upper mantle. Since crustal thermal weakening and lithospheric thinning occur above the asthenospheric wedge (Isacks, 1988), a shallow-dipping subducting plate may have been present during the Famatinian orogeny (Willner et al., 1987). During the exhumation period I (10^{-1} mm/yr), this crustal segment was exhumed to the upper crust, where it was intruded by supracrustal plutons (e.g. CBG) in Middle/Late Ordovician times (Fig. 9b). The crustal segment resided ~100 Myr in the upper crust without significant exhumation during period II (10^{-2} mm/yr) and was eventually intruded by post-tectonic plutons in Devonian/Carboniferous times (Fig. 9c). The erosion surface corresponds to the Carboniferous/Permian unconformity between Famatinian plutons and overlying continental sediments (e.g. Pieroni and Georgieff, 2007). The two periods of exhumation would have been driven by erosion, the former directly associated with crustal deformation. The relatively rapid period I was probably the result of enhanced erosion associated with a high initial relief. The high initial relief may be reflecting strong pure and then simple shear deformation during thickening. As internal relief attenuated, erosional efficiency decreased and exhumation was significantly slower during the period II. Reduction of topography may have been related either to geodynamic processes (e.g. decrease in deformation rates) or climate changes. However, the long time scale over which our exhumation rates are averaged does not permit a reasonable distinction.

9. Conclusions

The combination of thermobarometry and U–Pb geochronology of igneous and metamorphic rocks of the eastern Sierra de Velasco permitted to infer the P–T evolution and exhumation history of a crustal segment of the Famatinian Belt from the Early Ordovician to the Early Carboniferous. P–T paths of the studied samples indicate isobaric heating and cooling of the crust related to long thermal residence and moderate to slow exhumation. We estimated a first period I of moderate Ordovician

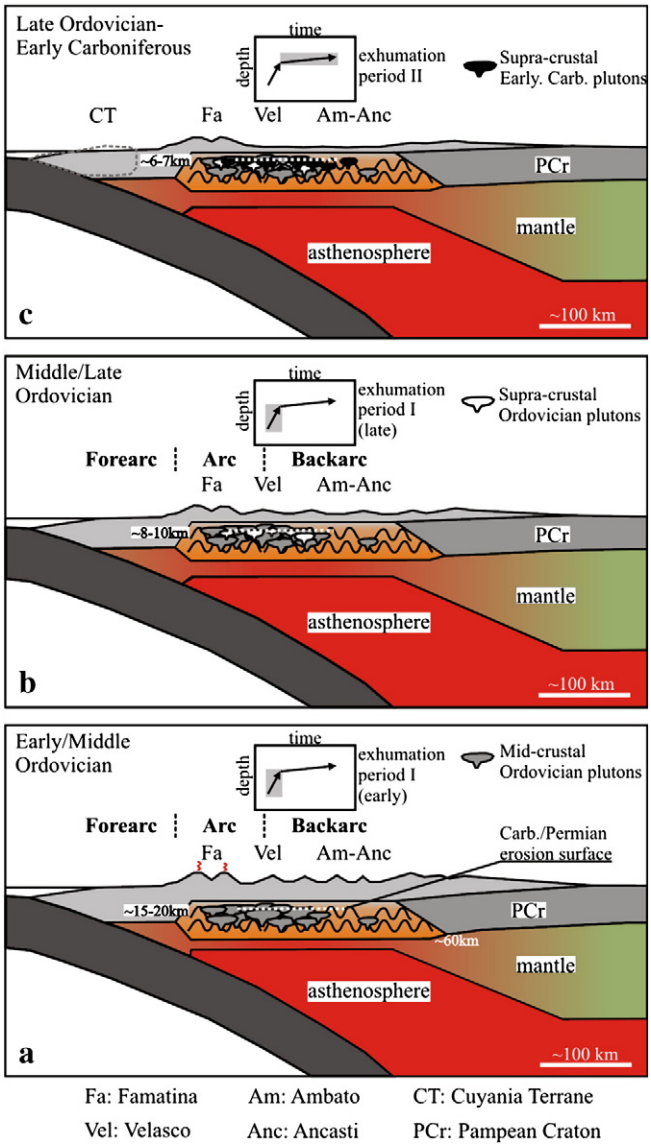

Fig. 9. Altiplano–Puna-like geodynamic evolution and erosion-dominated exhumation history of the Famatinian belt at the latitude of the study area. See further explanations in text.

exhumation rate and a second period of slow exhumation rate for the Sierra de Velasco, both similar to worldwide mean erosion rates. Regional field observations suggest that exhumation rates of our study area are valid for a wide area of the Famatinian Belt. Evidence such as widespread homogeneous exhumation associated with crustal thickening under a HT regime support the hypothesis that the Famatinian Belt represents the middle crust of an ancient Altiplano–Puna-like orogen. The lack of regional evidence for ductile thinning or normal faulting suggests that erosion was the primary exhumation mechanism, as occurs in most part of the Andean orogen. The evolution of the present-day exposed Famatinian Belt at the latitude of the Sierra de Velasco and neighbouring regions started in the middle crust, where high heat input combined with ductile compressive deformation led to strong crustal thickening. Lithospheric thinning over a shallow-dipping subducting plate, probably caused by asthenospheric removal of the upper mantle, caused widespread HT/MP conditions in the middle crust characterized by migmatization coeval with magmatic activity at ~475–480 Ma. The thermal regime of the Famatinian Belt ended at ~340–360 Ma with the intrusion of post-tectonic plutons in the upper crust. Exhumation of a deformation-driven high-relief Famatinian main- and back-arc was faster during the Ordovician (~0.25–0.78 mm/yr). Subsequently, reduction of topography caused a decrease in erosion efficiency and consequent slower exhumation rates between the Middle/Late Ordovician and the Early Carboniferous (~0.01–0.09 mm/yr). Complete exhumation of the Famatinian Belt in the Sierra de Velasco occurred near the Carboniferous/Permian limit, as indicated by continental sediments directly overlying the studied plutons. In summary, we interpret that the Famatinian belt was first moderately-fast and then slowly exhumed from the middle crust by erosion in ~180 Myr, which decreased as relief attenuated at the end of the Famatinian orogeny.

Acknowledgements

This work was funded by CONICET Grant no. PICT 0159, ANPCyT PICT Grant no. 07-09686, and CIUNT Grant no. 26-G222. CONICET and DAAD are thanked for scholarships awarded to C. R. de los Hoyos during his PhD studies. Technical support from INSUGEO-CONICET, Universidad Nacional de Tucumán, CPGeo-Universidade de Sao Paulo, and Ruhr-Universität in the preparation of this work is acknowledged. The fruitful teaching and support of Dr. Heinz-Jürgen Bernhardt on the use of the electron microprobe are gratefully thanked. We thank editors E. Tohver and M. Santosh for editorial guidance as well as J. Barnes and two anonymous reviewers for their constructive reviews.

Appendix A. Supplementary data

Supplementary materials related to this article can be found online at doi:10.1016/j.coastaleng.2010.12.002.

References

Aceñolaza, F., Toselli, A., 1973. Consideraciones estratigráficas y tectónicas sobre el paleozoico inferior del noroeste argentino. 2° Congreso Latinoamericano de Geología, vol. 2, pp. 755–763. Caracas.
Alasino, P.H., Dahlquist, J.A., Galindo, C., Casquet, C., Saavedra, J., 2009. Andalusite and Na- and Li-rich cordierite in the La Costa pluton, Sierras Pampeanas, Argentina: textural and chemical evidence for a magmatic origin. International Journal of Earth Sciences. doi:10.1007/s00531-009-0445-1.
Báez, M.A., Bellos, L.I., Grosse, P., Sardi, F.G., 2005. Caracterización petrológica de la sierra de Velasco. In: Dahlquist, J.A., Baldo, E.G., Alasino, P.H. (Eds.), Geología de la provincia de La Rioja, Precámbrico–Paleozoico Inferior: Asociación Geológica Argentina, Serie D, Publicación Especial, vol. 8, pp. 123–130.
Barnes, J.B., Ehlers, T.A., 2009. End member models for Andean Pleateau uplift. Earth Science Reviews 97, 117–144.
Bellos, L.I., 2005. Geología del sector sur de la sierra de Velasco, La Rioja. In: Aceñolaza, F., Aceñolaza, G., Hünicken, M., Rossi, J., Toselli, A. (Eds.), Simposio Bodenbender. INSUGEO: Serie Correlación Geológica, vol. 19, pp. 261–278.
Berman, R., 1991. Thermobarometry using multiequilibrium calculations: a new technique, with petrological applications. Canadian Mineralogist 29, 833–855.
Brown, M., 2010. Paired metamorphic belts revisited. Gondwana Research 18, 46–59.
Bucher, K., Frey, M., 1994. Petrogenesis of Metamorphic Rocks. Springer-Verlag, Berlin, Heidelberg.
Büttner, S., Glodny, J., Lucassen, F., Wemmer, K., Erdmann, S., Handler, R., Franz, G., 2005. Ordovician metamorphism and plutonism in the Sierra de Quilmes metamorphic complex: implications for the tectonic setting of the Northern Sierras Pampeanas (NW Argentina). Lithos 83, 143–181.
Büttner, S.H., 2009. The Ordovician Sierras Pampeanas–Puna basin connection: basement thinning and basin formation in the Proto-Andean back-arc. Tectonophysics 477, 278–291.
Castro de Machuca, B., Arancibia, G., Morata, D., Belmar, M., Previley, L., Pontoriero, S., 2008. P–T–t evolution of an Early Silurian medium-grade shear zone on the west side of the Famatinian magmatic arc, Argentina: implications for the assembly of the Western Gondwana margin. Gondwana Research 13, 216–226.
Conolly, J., 1990. Multivariable phase diagrams: an algorithm based on generalized thermodynamics. American Journal of Sciences 290, 666–718.
Dahlquist, J.A., Baldo, E.G., 1996. Metamorfismo y deformación famatinianos en la Sierra de Chepes, La Rioja, Argentina. XIII Congreso Geológico Argentino y III Congreso de Exploración de Hidrocarburos 5, 393–409.
Dahlquist, J.A., Rapela, C.W., Baldo, E.G., 2005. Petrogenesis of cordierite-bearing S-type granitoids in Sierra de Chepes, Famatinian Orogen, Argentina. Journal of South American Earth Sciences 20, 231–251.
Dahlquist, J.A., Pankhurst, R.J., Rapela, C.W., Casquet, C., Fanning, C.M., Alasino, P., Báez, M., 2006. The San Blas Pluton: an example of Carboniferous plutonism in the Sierras Pampeanas, Argentina. Journal of South American Earth Sciences 20, 341–350.
Dahlquist, J.A., Pankhurst, R.J., Rapela, C.W., Galindo, C., Alasino, P., Fanning, C.M., Saavedra, J., Baldo, E., 2008. New SHRIMP U–Pb data from the Famatina Complex:

constraining Early-Mid Ordovician Famatinian magmatism in the Sierras Pampeanas, Argentina. Geologica Acta 6 (4), 319–333.
Delpino, S.H., Bjerg, E.A., Ferracutti, G.R., Morgessie, A., 2007. Counterclockwise tectono-metamorphic evolution of the Pringles Metamorphic Complex, Sierras Pampeanas of San Luis (Argentina). Journal of South American Earth Sciences 23, 147–175.
Ehlers, T.A., 2005. Crustal thermal processes and the interpretation of thermochronometer data. In: Reiners, P.W., Ehlers, T.A. (Eds.), Low-temperature Thermochronology: Techniques, Interpretations and Applications. Mineralogical Society of America, pp. 315–350.
Fernández, C., Becchio, R., Castro, A., Viramonte, J.M., Moreno-Ventas, I., Corretgé, L.G., 2008. Massive generation of atypical ferrosilicic magmas along the Gondwana active margin: implications for cold plumes and back-arc magma generation. Gondwana Research 14, 451–473.
Foster, G., Gibson, H.D., Parrish, R., Horstwood, M., Fraser, J., Tindle, A., 2000. Textural, chemical and isotopic insights into the nature and behaviour of metamorphic monazite. Chemical Geology 191, 183–207.
Gaidies, F., Krenn, E., De Capitani, C., Abart, R., 2008. Coupling forward modelling of garnet growth with monazite geochronology: an application to the Rappold Complex (Austroalpine crystalline basement). Journal of Metamorphic Geology 19, 775–793.
Gilbert, H., Beck, S., Zandt, G., 2006. Lithospheric and uppermantle structure of central Chile and Argentina. Geophysical Journal International 165, 383–398.
González Bonorino, F., 1951. Una nueva formación Precámbrica en el noroeste Argentino. Comunicaciones Científicas, Museo de La Plata 5, 4–6.
Grosse, P., Sardi, F.G., 2005. Geología de los granitos Huaco y Sanagasta, sector centro-oriental de la Sierra de Velasco, La Rioja. In: Aceñolaza, F., Aceñolaza, G., Hünicken, M., Rossi, J., Toselli, A. (Eds.), Simposio Bodenbender. INSUGEO: Serie Correlación Geológica, 19, pp. 221–238.
Grosse, P., Söllner, F., Báez, M.A., Toselli, A.J., Rossi, J.N., De La Rosa, J.D., 2009. Lower Carboniferous post-orogenic granites in central-eastern Sierra de Velasco, Sierras Pampeanas, Argentina: U–Pb monazite geochronology, geochemistry and Sr–Nd isotopes. International Journal of Earth Sciences 98 (5), 1001–1025.
Hauzenberger, C.A., Morgessie, A., Hoinkes, G., Felfernig, A., Bjerg, E.A., Kostadinoff, J., Delpino, S.H., Dimitri, L., 2001. Metamorphic evolution of the Sierras de San Luis, Argentina: granulite facies metamorphism related to mafic intrusions. Mineralogy and Petrology 71, 95–126.
Heit, B., Koulakov, I., Asch, G., Yuan, X., Kind, R., Alcocer-Rodriguez, I., Tawackoli, S., Wilke, H., 2008. More constraints to determine the seismic structure beneath the Central Andes at 21° S using teleseismic tomography analysis. Journal of South American Earth Sciences 25, 22–36.
Höckenreiner, M., Söllner, F., Miller, H., 2003. Dating the TIPA shear zone: an Early Devonian terrane boundary between Famatinian and Pampean systems (NW-Argentina). Journal of South American Earth Sciences 16 (1), 45–66.
Holdaway, M.J., 2000. Application of new experimental and garnet Margules data to the garnet-biotite geothermometer. American Mineralogist 85, 881–892.
Holland, T.J.B., Powell, R., 1998. An internally consistent thermodynamic data set for phases of petrological interest. Journal of Metamorphic Geology 16, 309–343.
Holland, T.J.B., 2002. Index of Solid Solution Model and Internally Consistent Dataset. University of Cambridge, Department of Earth Sciences. From Holland, T.J.B. web site http://www.esc.cam.ac.uk/astaff/holland/ds5.
Isacks, B.L., 1988. Uplift of the Central Andean Plateau and bending of the Bolivian Orocline. Journal of Geophysical Research 93 (B4), 3211–3231.
Larrovere, M., Toselli, A., Rossi de Toselli, J., 2008. Petrología y estructura de la Faja de Deformación La Chilca, Catamarca, Argentina. Revista de la Asociación Geológica Argentina 63 (2), 254–263.
Larrovere, M.A., de los Hoyos, C.R., Toselli, A.J., Rossi, J.N., Basei, M.A.S., Belmar, M.E., 2011. High T/P evolution and metamorphic ages of the migmatitic basement of northern Sierras Pampeanas, Argentina: characterization of a mid-crustal segment of the Famatinian belt. Journal of South American Earth Sciences 31, 279–297.
Le Corre, C., Rossello, E., 1994. Kinematics of early Paleozoic ductile deformation in the basement of NW Argentina. Journal of South American Earth Sciences 7, 301–308.
López, J., Toselli, A., 1993. La faja milonítica Tipa: faldeo oriental del Sistema de Famatina, Argentina. XII Congreso Geologico Argentino, Mendoza. Actas 3, 39–42.
Lucassen, F., Becchio, R., Wilke, H.G., Thirlwall, M.F., Viramonte, J., Franz, G., Wemmer, K., 2000. Proterozoic–Paleozoic development of the basement af the Central Andes (18°–26°) — a mobile belt of the South America craton. Journal of South American Earth Sciences 13, 697–715.
Lucassen, F., Becchio, R., 2003. Timing of high-grade metamorphism: Early Palaeozoic U–Pb formation ages of titanite indicate long-standing high-T conditions at the western margin of Gondwana (Argentina, 26–29°S). Journal of Metamorphic Geology 21, 649–662.
Lucassen, F., Franz, G., 2005. The early paleozoic orogen in the central Andes: a non-collisional orogen comparable to the cenozoic high plateau? In: Vaughan, A., Leat, P., Pankhurst, R. (Eds.), Terrane Processes at the Margins of Gondwana: Geological Society of London, Special Publications, vol. 246, pp. 257–373.
Ludwig, K.R., 2003. User's manual for Isoplot 3.0: a geochronological toolkit for Microsoft Excel. Berkeley Geochronology Center, Special Publication, vol. 4. 71 pp.
Martina, F., Viramonte, J.M., Astini, R.A., Pimentel, M.M., Dantas, E., 2010. Mississippian volcanism in the south-central Andes: new U–Pb SHRIMP zircon geochronology and whole rock geochemistry. Gondwana Research. doi:10.1016/j.gr.2010.07.004.
Maruyama, S., Masago, H., Katayama, I., Iwase, Y., Toriumi, M., Omori, S., Aoki, K., 2010. A new perspective on metamorphism and metamorphic belts. Gondwana Research 18, 106–137.
Massonne, H.J., Schreyer, W., 1987. Phengite geobarometry based on the limiting assemblage with K-feldspar, phlogopite and quartz. Contributions to Mineralogy and Petrology 96, 212–224.
Milliman, J.D., Syvitski, J.P.M., 1992. Geomorphic/tectonic control of sediment discharge to the ocean: the importance of small mountainous rivers. Journal of Geology 100, 525–544.
Mirwald, P.W., Scola, M., Tropper, P., 2008. Experimental study on the incorporation of Na in Mg-cordierite in the presence of different fluids (Na (OH), NaCl–H_2O, albite-H_2O). Geophysical Research Abstracts 10 SRef-ID: 1607-7962/gra/EGU2008-A-04149.
Miyashiro, A., 1994. Metamorphic Petrology. University College of London, London. 404 pp.
Otamendi, J.E., Castellarini, P.A., Fagiano, M.R., Demichelis, A.H., Tibaldi, A.M., 2004. Cambrian to Devonian geologic evolution of the Sierra de Comechingones, Eastern Sierras Pampeanas, Argentina: evidence for the development and exhumation of continental crust on the Proto-Pacific margin of Gondwana. Gondwana Research 7 (4), 1143–1155.
Otamendi, J.E., Tibaldi, A.M., Vujovich, G.I., Viñao, G.A., 2008. Metamorphic evolution of migmatites from the deep Famatinian arc crust exposed in Sierras Valle Fértil-La Huerta, San Juan, Argentina. Journal of South American Earth Sciences 25, 313–335.
Pankhurst, R., Rapela, C., Saavedra, J., Baldo, E., Dahlquist, J., Pascua, I., Fanning, C., 1998. The Famatinian magmatic arc in the Central Sierras Pampeanas: an early to mid-Ordovician continental arc on the Gondwana margin. In: Pankhurst, R., Rapela, C. (Eds.), The Proto-Andean Margin of Gondwana: Geological Society of London, Special Publications, vol. 142, pp. 343–367.
Pankhurst, R., Rapela, C., Fanning, C., 2000. Age and origin of coeval TTG, I- and S-type granites in the Famatinian belt of NW Argentina. Transactions of the Royal Society of Edinburgh: Earth Sciences 91, 151–168.
Parrish, R.R., 1990. U–Pb dating of monazite and its application to geological problems. Canadian Journal of Earth Sciences 27, 1431–1450.
Patiño Douce, A.E., Harris, N., 1998. Experimental constraints on Himalayan anatexis. Journal of Petrology 39 (4), 689–710.
Pieroni, E.M., Georgieff, S.M., 2007. Reconsideración estratigráfica del Neopaleozoico de los alrededores del dique Los Sauces, La Rioja. Revista de la Asociación Geológica Argentina 62, 105–115.
Rapela, C.W., Coira, B., Toselli, A., Saavedra, J., 1992. The lower Paleozoic magmatism of southwestern Gondwana and the evolution of Famatinian orogen. International Geology Review 34, 1142–1181.
Rapela, C., Pankhurst, R., Baldo, E., Casquet, C., Galindo, C., Fanning, C., Saavedra, J., 2001. Ordovician metamorphism in the Sierras Pampeanas: new U–Pb SHRIMP ages in central-east Valle Fértil and the Velasco Batolith. III Simposio Sudamericano de Geología Isotópica 1, 611–614.
Reddy, S.M., Wheeler, J., Cliff, R.A., 1999. The geometry and timing of orogenic extension: an example from the western Italian Alps. Journal of Metamorphic Geology 17, 573–589.
Ring, U., Brandon, M.T., Willett, S.D., Lister, G.S., 1999. Exhumation processes. In: Ring, U., Brandon, M.T., Lister, G.S., Willett, S.D. (Eds.), Exhumation Processes: Normal Faulting, Ductile Flow and Erosion: Geological Society of London, Special Publications, vol. 154, pp. 1–27.
Rossi, J.N., Toselli, A.J., López, J.P., 1999. Deformación y metamorfismo en el NW de la sierra de Velasco, La Rioja, Argentina. Zentralblatt für Geologie und Paläontologie I (7/8), 839–850.
Rossi, J.N., Toselli, A.J., Saavedra, J., Sial, A.N., Pellitero, E., Ferreira, V.P., 2002. Common crustal source for contrasting peraluminous facies in the Early Paleozoic Capillitas Batholith, NW Argentina. Gondwana Research 5, 325–337.
Rossi, J.N., Toselli, A.J., Báez, M.A., 2005. Evolución termobárica del ortogneis peraluminoso del noroeste de la sierra de Velasco, La Rioja. Revista de la Asociación Geológica Argentina 60, 278–289.
Rossi, J.N., Toselli, A.J., 2005. Termobarometría de las corneanas granatíferas del flanco sudoccidental de la sierra de Velasco. La Rioja, Argentina. In: Aceñolaza, F.G., Aceñolaza, G., Hünicken, M., Rossi, J.N., Toselli, A.J. (Eds.), Simposio Bodenbender: Serie Correlación Geológica, vol. 19, pp. 248–259.
Rubatto, D., Hermann, J., Buick, I.S., 2006. Temperature and bulk composition control on the growth of Monazite and zircon during low-pressure anatexis (Mount Stafford, Central Australia). Journal of Petrology 47 (10), 1973–1996.
Saavedra, J., Toselli, A.J., Rossi, J.N., Pellitero, E., Durand, F., 1998. The Early Paleozoic magmatic record of the Famatina system: a review. In: Pankhurst, R.J., Rapela, C.W. (Eds.), The Proto-Andean Margin of Gondwana: Geological Society of London, Special Publication, 142, pp. 283–295.
Schärer, U., 1984. The effect of initial ^{230}Th disequilibrium on young U–Pb ages: the Makalu case, Himalaya. Earth and Planetary Science Letters 67, 191–204.
Scherrer, N.C., Engi, M., Gnos, E., Jakob, V., Liechti, A., 2000. Monazite analysis; from sample preparation to microprobe age dating and REE quantification. Schweizerische Mineralogische und Petrographische Mitteilungen 80, 93–105.
Schurr, B., Rietbrock, A., Asch, G., Kind, R., Oncken, O., 2006. Evidence for lithospheric detachement in the Central Andes from local earthquake topography. Tectonophysics 415, 203–223.
Siivola, J., Schmid, R., 2007. List of Mineral Abbreviations. SCMR website Recommendations by the IUGS Subcommission on the Systematics of Metamorphic Rocks. www.bgs.ac.uk/SCMR. version 01.02.07.
Spear, F.S., Cheney, J.T., 1989. A petrogenetic grid for pelitic schists in the system SiO_2–Al_2O_3–FeO–MgO–K_2O–H_2O. Contributions to Mineralogy and Petrology 101, 149–164.
Steenken, A., Siegesmund, S., Lopez de Luchi, M., Frei, R., Wemmer, K., 2006. Neoproterozoic to Early Palaeozoic events in the Sierra de San Luis: implications for the Famatinian geodymamics in the Eastern Sierras Pampeanas (Argentina). Journal of the Geological Society of London 163, 965–982.
Steiger, R., Jäeger, E., 1977. Subcommission on geochronology: convention on the use of decay constants in geo- and cosmochronology. Earth and Planetary Science Letters 36, 359–362.
Thompson, A.B., 1982. Dehydration melting of pelitic rocks and the generation of H_2O-undersaturated granitic liquids. American Journal of Science 282, 1567–1595.
Tortello, M.F., Esteban, S.B., 2007. Trilobites de la Formación Volcancito (Miembro Filo Azul, Cámbrico Tardío) del Sistema de Famatina, La Rioja, Argentina: aspectos sistemáticos y paleoambientales. Ameghiniana 44 (3), 597–620.

Toselli, A.J., Durand, F.R., Rossi de Toselli, J.N., Saavedra, J., 1996. Esquema de la evolución geotectónica y magmática Eopaleozoica del sistema de Famatina y sectores de Sierras Pampeanas. XIII Congreso Geológico Argentino y III Congreso de Exploración de Hidrocarburos 5, 443–462.

Verdecchia, S.O., Baldo, E.G., 2010. Geoquímica y procedencia de los metasedimentos ordovícicos del complejo metamórfico La Cébila, provincia de La Rioja, Argentina. Revista Mexicana de Ciencias Geológicas 27 (1), 97–111.

Vielzeuf, D., Holloway, J.R., 1988. Experimental determination of the fluid-absent melting relations in the pelitic system. Consequences for crustal differentiation. Contributions to Mineralogy and Petrology 98, 257–276.

Vujovich, G.I., 1994. Geología del basamento ígneo-metamórfico de la loma de Las Chacras, sierra de La Huerta, San Juan. Revista de la Asociación Geológica Argentina 49, 321–336.

Wegmann, M.I., Riller, U., Hongn, F.D., Glodny, J., Oncken, O., 2008. Age and kinematics of ductile deformation in the Cerro Durazno area, NW Argentina: significance for orogenic processes operating at the western margin of Gondwana during Ordovician–Silurian times. Journal of South American Earth Sciences 26, 78–90.

Whitmeyer, S.J., Simpson, C., 2004. Regional deformation of the Sierra de San Luis, Argentina: implications for the Paleozoic development of western Gondwana. Tectonics 23. doi:10.1029/2003TC001542.

Whitney, D.L., Irving, J.A., 1994. Origin of K-poor leucosomes in a metasedimentary migmatite complex by ultrametamorphism, syn-metamorphic magmatism and subsolidus processes. Lithos 32, 173–192.

Willner, A.P., Lottner, U.S., Miller, H., 1987. Early Paleozoic structural development in the NW Argentine basement of the Andes and its implication for geodynamic reconstructions. In: McKenzie, G.D. (Ed.), Gondwana Six: Structure, Tectonics and Geophysics. American Geophysical Union, pp. 229–239.

Willner, A.P., Thomson, S.N., Kröner, A., Wartho, J.A., Wijbrans, J.R., Hervé, F., 2005. Time markers for the evolution and exhumation history of a Late Palaeozoic paired metamorphic belt in North-Central Chile (34°–35°30′ S). Journal of Petrology 46 (9), 1835–1858.

Wu, C.M., Zhang, J., Ren, L.D., 2004. Empirical garnet–biotite–plagioclase–quartz (GBPQ) geobarometry in medium- to high-grade metapelites. Journal of Petrology 45, 1907–1921.

Wu, C.M., Zhao, G.C., 2007. The metapelitic garnet–biotite–muscovite–aluminosilicate–quartz (GBMAQ) geobarometer. Lithos 97, 365–372.